

Superradiant growth anomaly magnification in evolution of vector bosonic condensates bounded by a Kerr black hole with near-horizon reflection

Nayun Jia,^{1,2,*} Yin-Da Guo,^{3,†} Gui-Rong Liang,^{1,4,‡} Zhan-Feng Mai,^{5,6,§} and Xin Zhang^{2,7,8,¶}

¹*Department of Physics, Southern University of Science and Technology, Shenzhen 518055, China*

²*Key Laboratory of Cosmology and Astrophysics (Liaoning) & College of Sciences,
Northeastern University, Shenyang 110819, China*

³*Institute of Frontier and Interdisciplinary Science,
Key Laboratory of Particle Physics and Particle Irradiation (Ministry of Education),
Shandong University, Qingdao 266237, China*

⁴*School of Materials Science and Physics, China University of Mining and Technology, Xuzhou 221116, China*

⁵*Kavli Institute for Astronomy and Astrophysics, Peking University, Beijing 100871, China*

⁶*Guangxi Key Laboratory for Relativistic Astrophysics,
School of Physical Science and Technology,
Guangxi University, Nanning 530004, China*

⁷*Key Laboratory of Data Analytics and Optimization for Smart Industry (Ministry of Education),
Northeastern University, Shenyang 110819, China*

⁸*National Frontiers Science Center for Industrial Intelligence and Systems Optimization,
Northeastern University, Shenyang 110819, China*

Ultralight vector particles can form evolving condensates around a Kerr black hole (BH) due to superradiant instability. We study the effect of near-horizon reflection on the evolution of this system: by matching three pieces of asymptotic expansions of the Proca equation in Kerr metric and considering the leading order in the electric mode, we present explicit analytical expressions for the corrected spectrum and the superradiant instability rates. Particularly, in high-spin BH cases, we identify an anomalous situation where the superradiance rate is temporarily increased by the reflection parameter \mathcal{R} , which also occurs in the scalar scenario, but is largely magnified in vector condensates due to a faster growth rate in dominant mode. We point out the condition for the growth anomaly in the adiabatic case is that information carried per particle exceeds a certain value $\delta I/\delta N > 2\pi k_B \sqrt{(1+\mathcal{R})/(1-\mathcal{R})}$. We further construct several featured quantities to illustrate it, and formalize the anomaly-induced gravitational wave strain deformation.

* nayun.jia@foxmail.com

† yinda.guo@mail.sdu.edu.cn

‡ Corresponding author: blueigr@sina.com

§ zhanfeng.mai@gmail.com

¶ zhangxin@mail.neu.edu.cn

CONTENTS

I. Introduction	3
II. Hydrogenic spectrum for vector bosonic condensates and Proca equation in Kerr spacetime	7
A. Hydrogenic solutions in non-relativistic approximation and spectrums	9
B. Analytical description with separable ansatz and leading order behaviors	12
C. Matching three pieces of asymptotic expansions in the radial function	14
III. The corrected spectrums with near-horizon reflection and superradiant growth anomaly	18
A. Reflective boundary conditions near the horizon and corrected superradiance rate	18
B. The superradiance modifier and the growth anomaly conditions	22
IV. Effects of reflection on the BH-condensate evolution and anomaly features	25
A. General evolutions and final state estimates	25
B. Anomaly features and GW strain magnification	30
V. Conclusion and discussion	33
Acknowledgements	35
References	35

I. INTRODUCTION

Ultralight bosonic particles, which are promising predictions in a variety of beyond-Standard-Model theories [1–6] have caught much attention as competitive candidates for dark matter [7–19]. They originally arise from the Peccei-Quinn axion [20] introduced to solve the strong CP problem, and later enlarged to include familions [21] and Majorons [22] from spontaneous symmetry breaking; string theory could even suggest simultaneous presence of numerous axion-like particles taking up the mass spectrum down to the Planck mass [23], filling the gap between observed massless and very massive elementary bosons. Effective scalar degrees of freedom can also naturally arise from several modified theories of gravity [24, 25]. In addition to scalar/pseudo-scalar fields, the zoo of light bosons extends to those with spin: massive vector fields, or known as dark photons [26, 27], arise in the hidden U(1) sector [28–32]; massive tensor fields, with the potential to modify the gravitational interaction at large scale, could possibly account for the acceleration of cosmic expansion [33, 34]. While traditional detections of such ultralight bosonic particles in laboratory are extremely challenging, their Bose-Einstein condensates around a massive Black Hole (BH), via the mechanism of superradiance, may provide interesting phenomenology and possible observations at astrophysical and cosmological scales [23, 35].

Superradiance, which is a well-known phenomenon in flat spacetime, exhibits the amplification of incoming energy and give it back outwards. Its rotational case manifestly show up in the tidal heating and acceleration in the Earth-Moon system, in which frictions between the Earth and the tidal bulge would at the same time transfer the energy to heat and lifts the Moon’s orbit [12]. Superradiance is a consequence of second law of thermodynamics, with dissipation the most essential ingredient. In BH physics, the effect of dissipation is induced by the ergosphere, where spacetime is dragged like the tidal bulge; this “viscous region” makes the energy extraction from BHs possible, known as the Penrose process, with its wave analog amplifies the magnitude of incoming amplitude. The superradiance condition can be directly given by the BH area theorem, although the logic is originally reverse. The BH first law relates its change in mass M , angular momentum J , horizon area A , in the rotational but neutral case as

$$\delta M = \frac{\kappa}{8\pi} \delta A + \Omega_H \delta J \quad (1)$$

with κ the surface gravity and Ω_H the horizon angular velocity. A wave with frequency ω and an azimuthal number m carried away gives rise to the BH angular momentum and mass loss ratio as

$\delta J/\delta M = m/\omega$, this reshapes the above first law as

$$\delta A = \frac{8\pi}{\kappa} \frac{(\omega - m\Omega_H)}{\omega} \delta M, \quad (2)$$

joining with the second law $\delta A > 0$ and the mass loss in BH $dM < 0$ requires

$$\omega < m\Omega_H, \quad (3)$$

which is the superradiance condition. However, if the amplification happens only once, the back-reaction to the spacetime is verified to be at second orders of perturbation [12, 36], i.e., the spacetime is stable. The instability occurs when a reflective boundary is put far from the BH, bouncing the outgoing waves back to the BH over and over again, which can be achieved by putting a mirror in toy models [37, 38], or in AdS spacetimes [39–41]; while in realistic astrophysical contexts, the mass of the boson itself serves as a natural mirror to confine its distribution range, thus forming a quasi-bounded system, known as a “gravitational atom” [42], featured with a “gravitational fine structure constant”. The constant is taken from atomic physics by dividing $\hbar c$ into the coefficient of inverse square law,

$$\alpha \equiv \frac{GM\mu}{\hbar c} = \frac{r_g}{\lambda_c} = \frac{\lambda_c}{r_B} \simeq 0.02 \left(\frac{M}{3M_\odot} \right) \left(\frac{\mu}{10^{-12}\text{eV}} \right), \quad (4)$$

where μ is the boson mass considered to be a free parameter, with $\lambda_c = \hbar/\mu c$ the corresponding Compton wave length, $r_g = GM/c^2$ and $r_B = \hbar^2/(GM\mu^2)$ are the gravitational radius and the Bohr radius respectively. In such an atomic structure, the BH-boson system exhibits a hydrogen-like spectrum but with growing occupation numbers at each energy level. Predicted monochromatic gravitational waves (GW) are generated either from transitions or annihilations between or within these levels for a long period of time [42–63], potentially to put constraints on the physical parameters of these ultralight bosonic dark matters [64–70].

The growing condensate is characterized by the superradiance rate, for a bosonic state with spin- s , and in the limit of small mass coupling α , the rate [54, 59] scales as

$$\Gamma_{nljm} \propto (m\Omega_H - \omega) \alpha^{2(l+j)+5}, \quad (5)$$

with the orbital angular momentum l and the total angular momentum number $j \in (|l-s|, l+s) > 0$ integers, and $m \in (-j, j)$ the quantum projection of j along the rotation axis. The spins $s = 0, 1, 2$ are for scalar, vector, and tensor respectively. The superradiance condition (3) guarantees the positivity of the rate, otherwise the state becomes absorptive, which occurs definitely if $m = 0$ or possibly if bosons are too heavy bringing a large ω ; while too light bosons would lead to a much slower growth due to the

α -suppression. The optimal case occurs when $\omega \simeq \Omega_{\text{H}}$ and a BH is near-extremal, this gives $\alpha \simeq 0.5$ or equivalently $\lambda_c \simeq 2r_g$, which says when the bosonic Compton wavelength is around the radius of BH, the superradiance becomes most significant. In terms of different states, the largest rate occurs at smallest $(l + j)$ but maximum quantum number $m = j$, which will consequently lead to a larger GW amplitude during the superradiance. In Table I, we list several leading modes for scalar, vector and tensor field, according to different orbital angular momentum number l , for largest total angular momentum $j = l + s$ and largest quantum number $m = j$; and in Figure I, we plot schematic pictures of dominant scalar, vector and tensor modes around a spinning BH.

	$l=0$	$l=1$	$l=2$
Scalar: $ nlm\rangle_{(j=l)}$		$ 211\rangle$	$ 322\rangle$
Vector: $ nljm\rangle$	$ 1011\rangle$	$ 2122\rangle$	$ 3233\rangle$
Tensor: $ nljm\rangle$	$ 1022\rangle$	$ 2133\rangle$	$ 3244\rangle$

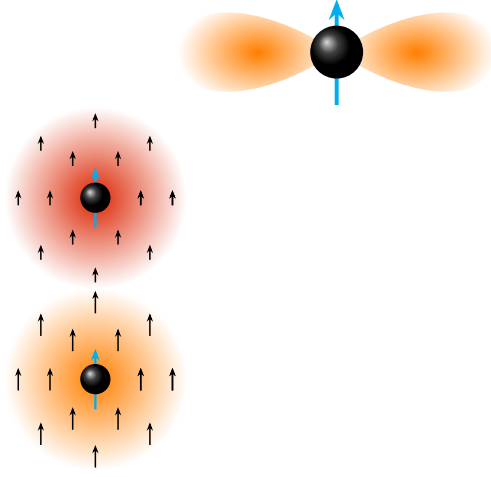


TABLE I. Leading superradiant states of different bosonic fields in terms of orbital angular momentum number l , for largest total angular momentum $j = l + s$ and largest quantum number $m = j$. The dominant modes are filled with colors, with the superior vector case $|1011\rangle$ in red, the following $|211\rangle$ and $|1022\rangle$ for scalar and tensor modes in orange, parallel to the left table fillings.

FIG. I. Schematic pictures of dominant scalar, vector and tensor modes around a spinning BH. The BH spins are denoted by blue arrows, the boson spins are denoted by black arrows; the superior vector condensate $|1011\rangle$ is in red, the following $|211\rangle$ and $|1022\rangle$ for scalar and tensor clouds are in orange, parallel to the left table fillings. The distribution for scalar is for $l = 1$, while those for vector and tensor are for $l = 0$; the arrows for tensors are 2 times as those of vectors.

It is clearly seen that the vector state $|1011\rangle$ with $l + j = 1$ has the largest growing rate, while both the scalar state $|211\rangle$ and the tensor state $|1022\rangle$ with $l + j = 2$ are α^2 orders of magnitude inferior¹. Further, a special feature of superradiantly-generated clouds with a vanishing orbital angular

¹ The only exception is the tensor polar dipole mode [51], growing uniquely with a non-hydrogenic form as $\Gamma \propto (m\Omega_{\text{H}} - \omega) \alpha^3$, which is beyond our current research scope.

momentum dominant growing mode, say $|1011\rangle$ or $|1022\rangle$, is that the distribution of the cloud is much closer to the BH horizon and the BH rotation energy is solely transferred into the bosonic intrinsic spin [42]; these makes the states especially sensitive to the near-horizon geometry of the BH. For these reasons, we highly suggest that the vector dominant state $|1011\rangle$ to serve as the best candidate to investigate phenomenology induced by near-horizon geometry, which is our main focus in this paper, see Fig. I. for a schematic picture.

The BH near-horizon geometry is trivial in classical theory of particle motions in general relativity, in which an event horizon is treated as one-way membrane where nothing can escape, superradiance in this case has been studied in different bosonic fields [71–75]. While the BH information paradox [76] suggests modifications near the BH horizon, which could be given in some semi-classical treatments of particle motions [77–83], or several quantum gravity theories [84–86]. The quantum-corrected models often involve these modifications by varying the boundary condition when a test field presents, with a reflection parameter \mathcal{R} introduced as an effective phenomenological description. This method is commonly employed in the study of GW echoes [87–95], and has been introduced to investigate possible effects on superradiance in scalar case in recent years [96–99]. But as we suggested earlier, the vector dominant state should be the best candidate to study near-horizon geometry, which is our focus in this paper. We will mainly investigate the influence of a real-valued reflection parameter \mathcal{R} on the superradiance rate $\Gamma(\mathcal{R})$ and draw possible conclusions on the evolution and the corresponding GW patterns.

The paper is organized as follows. In Section II, we employ the Proca field to describe the condensate around a Kerr BH; using a non-relativistic approximation, we obtain the hydrogenic spectrum of the vector field at a large distance from the BH, with a complexified frequency to include the superradiant mode of the quasibound BH-condensate system. In the leading-order of the angular part, the method of matched asymptotic expansions in radial part, in three pieces in our context, is used to obtain the analytical results. We optimize the matchings with near region solution by choosing a different basis, which provide simpler but natural connections to the boundary condition. In Section III, we introduce the reflection parameter describing a modified boundary condition at the horizon, and investigate its modifications to energy levels and the superradiance rate analytically. Particularly, in high-spin BH and low-frequency particle cases, the superradiance rate may temporally get boosted by the reflection, rather than monotonically being slowed down. This also occurs in scalar scenario, but is largely magnified in vector case due to the faster growth rate and closer distribution geometry, as shown in Table I

and in Figure I, and is named as an “anomaly” in our context. We give three forms of the anomaly condition, which have illustrative, geometrical, and physical meanings respectively, and point out this is due to a “rotation-relativistic” effect of fast-spinning BHs. In Section IV, we evaluate the influence of the reflection parameter on the whole system’s evolution, finding that the above “anomaly” only lasts temporally at the early stage, without affecting the final states too much, but it is most obvious in the vector case due to a overwhelming faster growth rate in dominant mode. This scenario is much like a version of “The Tortoise and the Hare”, with “the Tortoise” the normal decreasing superradiant rate with reflection, and “the Hare” the temporal anomalous superradiant boost. We introduce three featured quantities to describe the phenomenon: the maximum growth rate difference, the maximum condensate mass difference, and the advantage time of the anomaly. Further, we formalize the anomaly and estimate its effects on GW strain in the early stage. In Section V, we conclude our main procedure and results, followed by which a possible physical explanation for the anomaly is proposed, discussions and some extensions of the study are presented in the end. Throughout this paper, we adopt the Planck units $G_N = \hbar = c = 1$ and the $(+, -, -, -)$ signature, and a small coupling $\alpha = M\mu \ll 1$ approximation in the analytical analysis.

II. HYDROGENIC SPECTRUM FOR VECTOR BOSONIC CONDENSATES AND PROCA EQUATION IN KERR SPACETIME

In this section, we study the vector bosonic condensate around a Kerr black hole by solving the Proca equation in a Kerr metric; we will firstly demonstrate its non-relativistic approximate solutions in distant region from the horizon which exhibits hydrogenic features, then we will elaborate the full analytical treatment of matched asymptotics for the radial part, by considering the leading order of electric mode in the separated angular function.

The vector condensate is described by a free massive spin-1 field A_μ , the corresponding Lagrangian in an arbitrary spacetime is given by

$$\mathcal{L}_A = -\frac{1}{4}F_{\rho\sigma}F^{\rho\sigma} + \frac{1}{2}\mu^2 A_\gamma A^\gamma, \quad (6)$$

with μ the particle mass and the associated field tensor as

$$F_{\rho\sigma} \equiv \nabla_\rho A_\sigma - \nabla_\sigma A_\rho, \quad (7)$$

where indices are raised and lowered by the metric $g_{\rho\sigma}$.

Taking the Euler-Lagrangian equation for A^μ , the resulting Proca equation of motion (EoM) is

$$\nabla_\rho F^{\rho\sigma} + \mu^2 A^\sigma = 0, \quad (8)$$

with the Lorenz gauge condition $\nabla_\rho A^\rho = 0$ automatically satisfied; the EoM and gauge condition together constrain components of A^μ to have 3 independent degrees of freedom, which we choose to be the spatial components afterwards. The information of energy and momentum density and flux is encoded in the corresponding stress-energy tensor, which is given by

$$T_{\rho\sigma} = F_{\rho\lambda} F_\sigma{}^\lambda - \mu^2 A_\rho A_\sigma + g_{\rho\sigma} \left(-\frac{1}{4} F_{\alpha\beta} F^{\alpha\beta} + \frac{1}{2} \mu^2 A_\gamma A^\gamma \right). \quad (9)$$

In the superradiance regime, the black hole rotation triggers the bosonic condensate cloud growth; the most common astrophysical rotating Kerr BHs are dressed with only two distinguished features: the mass M and the angular momentum J , the corresponding metric in Boyer-Lindquist coordinates takes the form

$$\begin{aligned} ds^2 = & \left(1 - \frac{2Mr}{\Sigma} \right) dt^2 + \frac{4aMr}{\Sigma} \sin^2 \theta \, dt d\varphi - \frac{\Sigma}{\Delta} dr^2 - \Sigma d\theta^2 \\ & - \left[(r^2 + a^2) \sin^2 \theta + 2 \frac{Mr}{\Sigma} a^2 \sin^4 \theta \right] d\varphi^2, \end{aligned} \quad (10)$$

with

$$\begin{cases} \Delta \equiv r^2 - 2Mr + a^2, \\ \Sigma \equiv r^2 + a^2 \cos^2 \theta, \end{cases} \quad (11)$$

and $a \equiv J/M$ the BH angular momentum per unit mass. We will also refer to the dimensionless spin parameter $\chi \equiv a/M = J/M^2$ as the “BH spin” in the following context.

The inner and outer horizons r_\pm and infinite redshift surfaces r_\pm^s of the Kerr BH are given by

$$\begin{cases} r_\pm = M \pm \sqrt{M^2 - a^2} \\ r_\pm^s = M \pm \sqrt{M^2 - a^2 \cos^2 \theta}. \end{cases} \quad (12)$$

The classical analogue of superradiance, Penrose process, happens in ergosphere between r_+ and r_+^s where negative energy trajectories exist; the different boundary conditions with or without reflection are chosen at the outer horizon r_+ , since the inner horizon r_- is not physically accessible. The angular velocity of the outer horizon is given by $\Omega_H \equiv a/2Mr_+ = \chi/2r_+$.

Note that the quasi-adiabatic approximation is assumed when we employ the stationary Kerr metric (10). The bosonic field is typically distributed over a very large volume, implying very small densi-

ties and consequent small backreaction effects. It is treated as perturbation on the Kerr BH, giving a dynamical contribution to the background with a very small timescale, compared to typical oscillation period of the boson field and the instability timescale [69]. In other words, the BH is soon going back to the stationary case after the perturbation in the previous time instant, before we can use it as a background to continue the superradiance at the next instant.

A. Hydrogenic solutions in non-relativistic approximation and spectrums

As a first step, we will present a preliminary investigation into the solutions using a non-relativistic approximation, since its fundamental structure would exhibit key features of the gravitational atom by highly similar analytical energy levels, which could be sources of monochromatic GWs with waveform potentially to be influenced by superradiance with reflections.

We consider the situation where the Compton wavelength $\lambda_{\text{Compton}} \sim \mu^{-1}$ of the vector particles is substantially larger than the gravitational radius $r_g \equiv M$ of the BH, or equivalently, the mass coupling of the BH-condensate system $\alpha \equiv M\mu$ is much less than 1, hence our considered region is restricted to be located distantly from the BH horizon. Under these conditions, the solutions to the Proca equation in the Kerr metric will exhibit nonrelativistic and hydrogen-like properties [42]. Hence, a single solution can be expressed in the following form [54]:

$$A^\rho(t, x) = \frac{1}{\sqrt{2\mu}} (\Psi^\rho(x) e^{-i\omega t} + \text{c.c.}). \quad (13)$$

For $r \gg r_g$, substituting Eq. (13) into the Proca equation (8), and approximating the metric tensor so that it has flat space-space components $g_{ij} = \eta_{ij}$ and vanishing off-diagonal components $g_{0i} = 0$, and only a nontrivial component g_{00} , we obtain the following approximate EoM:

$$(\omega^2 - \mu^2) \Psi^\rho \approx -\nabla^2 \Psi^\rho - \omega^2 (-1 + g^{00}) \Psi^\rho, \quad (14)$$

with the component $g^{00} \approx (1 - 2r_g/r)$ in the Kerr metric at $r \gg r_g$. The spatial change in Ψ^μ is gradual, resulting in non-relativistic momenta of the particles, so the frequency of the bound state is approximately equal to its mass, $\omega \approx \mu$, to the leading order in α ; thus the EoM further simplifies to a Schrödinger-type equation with a potential of $1/r$:

$$(\omega - \mu) \Psi^\rho \approx -\frac{\nabla^2}{2\mu} \Psi^\rho + \frac{\alpha}{r} \Psi^\rho. \quad (15)$$

As stated above, we choose the 3 independent degrees of freedom to be the spatial components, then the temporal component is determined by the Lorentz gauge condition. Given the spherically symmetric feature of the $1/r$ potential, the spatial components can be solved by separation of variables:

$$\Psi_i = R^{nl}(r)Y_i^{l,jm}(\theta, \varphi), \quad (16)$$

with $\{n, l, j, m\}$ the principle, orbital angular momentum, total angular momentum, and azimuthal angular momentum numbers respectively, and totally determine the vector eigenstates; note that the scalar eigenstates are determined only by three numbers $\{n, l, m\}$, since there're no intrinsic spin of the scalar cloud itself. The orbital angular momentum number l is taken to be from 0 to n , and denoted by {s, p, d, f...}. The “pure-orbital vector spherical harmonics” $Y_i^{l,jm}(\theta, \varphi)$ are eigenfunctions of the orbital angular momentum operator [54, 100], satisfying

$$-r^2 \nabla^2 Y_i^{l,jm} = l(l+1)Y_i^{l,jm}, \quad (17)$$

with j taken to be $j = l \pm 1, l$, due to the spin-1 nature of vector field. The 3 degrees of freedom of the vector field can thus be transferred to be this 3 values of the total angular momentum number; the $j = l \pm 1$ modes are known as the “electric modes” and the $j = l$ modes as the “magnetic modes”, classified by their parity features [42, 100]. In the later discussion of more rigorous treatment, we will only focus on the electric modes, due to its mathematical convenience and exemplariness.

The radial solutions $R^{nl}(r)$ are hydrogenic wavefunctions, which can be expressed in terms of the associated Laguerre polynomials $L_n^{2l+1}(r)$ as in [69],

$$R_{nl}(\tilde{r}) = \sqrt{\left(\frac{2}{\bar{n}r_a}\right)^3 \frac{n!}{2\bar{n}(\bar{n}+l)!}} e^{-\tilde{r}/2} \tilde{r}^l L_n^{2l+1}(\tilde{r}), \quad (18)$$

where we changed our variable to be $\tilde{r} \equiv 2r/(\bar{n}r_a)$, with $r_a = 1/(M\mu^2)$ the “Bohr radius” and principle quantum number $\bar{n} = n + l + 1$ labeling the “energy levels” of the system, analogous to their quantum mechanical counterparts. Thus we stated the non-relativistic approximation exhibits hydrogenic features in the beginning of this subsection; more explicitly, these levels are presented in a highly similar form with that of hydrogen atom

$$\omega \approx \mu \left(1 - \frac{\alpha^2}{2\bar{n}^2}\right), \quad (19)$$

where a higher order correction in α is added, to the leading order approximation $\omega \approx \mu$. Identification of these discrete energy levels allows two channels for monochromatic GW emission, from level transitions

or annihilations [64], with angular frequencies

$$\begin{cases} \omega_{\text{tr}} = \frac{1}{2}\mu\alpha^2 \left(\frac{1}{\bar{n}_{\text{H}}^2} - \frac{1}{\bar{n}_l^2} \right) \\ \omega_{\text{ann}} = 2\omega \simeq 2\mu \left(1 - \frac{\alpha^2}{2\bar{n}^2} \right), \end{cases} \quad (20)$$

with \bar{n}_{H} and \bar{n}_l principle quantum numbers of higher and lower energy levels.

More generally, in case of rotation, superradiant instability is given by a complex shift to the frequency of this Bohr-like spectrum as

$$\omega = \omega_0 + \delta\omega \equiv \mu \sqrt{1 - \frac{\alpha^2}{\nu^2}}, \quad (21)$$

where the shifted and complexified energy level is defined as $\nu \equiv \bar{n} + \delta\nu$ with $\delta\nu \in \mathbb{C}$, $|\delta\nu| \ll \bar{n}$, then the two parts of the spectrum are extracted as

$$\begin{cases} \omega_0 = \mu \left(1 - \frac{\alpha^2}{2\bar{n}^2} \right), \\ \delta\omega = \frac{M^2\mu^3}{\bar{n}^3} \delta\nu. \end{cases} \quad (22)$$

we see that ω_0 is just the Bohr-like spectrum in (19), and the complex shift $\delta\omega$ is controlled by the shift in energy levels $\delta\nu$. If we write the spectrum in explicit real and imaginary part as $\omega = E + i\Gamma$, with E the new energy spectrums and Γ the superradiant instability rate, we have

$$\begin{cases} E = \omega_0 + \text{Re}(\delta\omega) \\ \Gamma = \text{Im}(\delta\omega), \end{cases} \quad (23)$$

which is solely determined by $\delta\omega$ and hence by $\delta\nu$. Thus the information of both spectrum and superradiant growth is totally encoded in the complex energy level ν , containing any possible changes by various potential modifications. In the following contents, the main task is to determine $\delta\nu$ in case of boundary conditions with the near-horizon reflection parameter \mathcal{R} , and to discuss the effects on superradiant growth and BH-bosonic bound system evolution. Notably, the effect of reflection can be factor out as

$$\delta\nu(\mathcal{R}) = \delta\bar{\nu} \Phi(\mathcal{R}) \quad (24)$$

with $\Phi(\mathcal{R} = 0) = 1$, thus $\delta\bar{\nu}$ denotes the modification purely due to superradiant instability without any reflection, and later we will see that $\delta\bar{\nu}$ is a pure imaginary number hence so is $\delta\omega$; therefore, in case of no reflection, the energy spectrum is not changed, $E = \omega_0$, according to (23); even in case of reflection, if $\text{Re}(\delta\omega) \ll \omega_0$, we can treat the energy spectrum as unchanged, and focus on the superradiance part, which will be our case in the later analysis.

B. Analytical description with separable ansatz and leading order behaviors

The non-relativistic approximation provides a general energy spectrum of the Proca condensate, but by dropping the off-diagonal metric components, it lost the key ingredient of Kerr geometry — the rotation, which is essential to trigger superradiance. To formally treat the problem, one has to solve the equation by substituting the Proca equation (8) into the Kerr metric (10). However, it is the rotation that complicates the analytical resolution, since the Proca equation in the Kerr background seemingly presents an issue of separability [12]; several attempts were made to tackle the problem, including semi-analytical treatments [48, 49] or numerical efforts [42, 50, 55]; afterwards, by generalizing the tools in treating Maxwell equations [101, 102], a proper ansatz [57] was proposed, which we will adopt in our following treatments.

The ansatz that captures all of the electric modes of a vector field on Kerr background takes the form [42, 57]

$$A^\mu = B^{\mu\nu} \nabla_\nu Z, \quad \text{with} \quad Z(t, \mathbf{r}) = e^{-i\omega t + im\varphi} R(r) S(\theta), \quad (25)$$

with $R(r)$ and $S(\theta)$ the “radial function” and the “angular function” in terminology, respectively; their relations to the actual vector field configuration in the far zone is given in [42]. The polarization tensor $B^{\mu\nu}$ is defined through the equation

$$B^{\mu\nu} (g_{\nu\sigma} + i\lambda^{-1} h_{\nu\sigma}) = \delta_\sigma^\mu, \quad (26)$$

with λ generally a complex number, which will be referred to as the “angular eigenvalue”; and $h_{\mu\nu}$ is called the principal tensor [103] which generates the symmetries of the Kerr spacetime, with its explicit expression given in [42]. For the magnetic modes, an educated hypothesis [42] suggests the same energy level and superradiant instability rate of the vector field as those of the electric modes, thus we will focus only on electric modes in this paper.

With the separable ansatz, the differential equations that radial and angular functions satisfy are extracted. The angular equation takes the form

$$\frac{1}{\sin \theta} \frac{d}{d\theta} \left(\sin \theta \frac{dS}{d\theta} \right) + \left[\Lambda - \frac{m^2}{\sin^2 \theta} + \mu^{-2} \alpha^2 \chi^2 (\omega^2 - \mu^2) \cos^2 \theta \right] S = \frac{2\mu^{-2} \alpha^2 \chi^2 \cos \theta}{\lambda^2 q_\theta} \left(\sin \theta \frac{d}{d\theta} + \sigma \lambda \cos \theta \right) S, \quad (27)$$

with

$$\begin{cases} q_\theta \equiv 1 - \mu^{-2} \alpha^2 \chi^2 \lambda^{-2} \cos^2 \theta, \\ \sigma \equiv \omega + \mu^{-1} \alpha \chi \lambda^{-2} (m - \mu^{-1} \alpha \chi \omega), \\ \Lambda \equiv \mu^2 \lambda^2 - \sigma \lambda + 2\mu^{-1} \alpha \chi \omega m - \mu^{-2} \alpha^2 \chi^2 \omega^2. \end{cases} \quad (28)$$

Note that we keep the vector mass μ in the expression, which causes slight difference in expressions with those in [42]. The radial equation reads

$$\begin{aligned} \frac{d^2 R}{dr^2} + \left(\frac{1}{r - r_+} + \frac{1}{r - r_-} - \frac{1}{r - \hat{r}_+} - \frac{1}{r - \hat{r}_-} \right) \frac{dR}{dr} + \left[-\frac{\Lambda}{\Delta} - (\mu^2 - \omega^2) + \frac{P_+^2}{(r - r_+)^2} + \frac{P_-^2}{(r - r_-)^2} \right. \\ \left. - \frac{A_+}{(r_+ - r_-)(r - r_+)} + \frac{A_-}{(r_+ - r_-)(r - r_-)} - \frac{\lambda \sigma r}{\Delta(r - \hat{r}_+)} - \frac{\lambda \sigma r}{\Delta(r - \hat{r}_-)} \right] R = 0, \end{aligned} \quad (29)$$

with $\hat{r}_\pm \equiv \pm i\lambda$ depending on the angular eigenvalue, and

$$\begin{cases} \gamma^2 \equiv \frac{1}{4} (r_+ - r_-)^2 (\mu^2 - \omega^2), \\ \gamma_\pm^2 \equiv M^2 (\mu^2 - 7\omega^2) \pm M (r_+ - r_-) (\mu^2 - 2\omega^2), \\ P_\pm \equiv \frac{am - 2M\omega r_\pm}{r_+ - r_-}, \\ A_\pm \equiv P_+^2 + P_-^2 + \gamma^2 + \gamma_\pm^2. \end{cases} \quad (30)$$

The poles at $r = r_\pm$ are the same as that in scalar radial functions which can be solved by matching near and far region solutions, while the additional poles at $r = \hat{r}_\pm$ appear here in vector case makes the widths of the two regions narrower thus don't overlap, thus it's necessary to introduce an intermediate region to fill the gap, which we will do in detail in the following subsection.

It's useful to note that the superradiance condition $\omega < m\Omega_H$ guarantees the positivity of P_+ , which is re-organized as

$$P_+ = \frac{2Mr_+}{r_+ - r_-} (m\Omega_H - \omega) = \frac{m\chi}{2\sqrt{1 - \chi^2}} \left(1 - \frac{\omega}{m\Omega_H} \right) > 0, \quad (31)$$

making the ingoing and outgoing terms $z^{\pm i P_+}$ explicit, with z a rescaled radial coordinate in the following contexts; and in the second equator we further wrote it in terms of the BH spin χ and the ‘‘superradiance saturation’’ $\omega/m\Omega_H$, for later convenience. Also note that in the small α limit, $P_+ = P_-$.

To solve the coupled differential equations (27) and (29) systematically, expansions should be done by orders of the coupling constant α . But still, hydrogenic properties exhibit in the leading order and in the far zone. The expressions with higher-order corrections can be found in Ref. [42]. For the electric

modes, by dropping explicit terms of α in (27), and invoking $\omega \simeq \mu$, the leading-order approximation of the angular part is obtained as

$$\left[\frac{1}{\sin \theta} \frac{d}{d\theta} \left(\sin \theta \frac{d}{d\theta} \right) - \frac{m^2}{\sin^2 \theta} + \tilde{\lambda}_0 (\tilde{\lambda}_0 - 1) \right] S_0 = 0, \quad (32)$$

with $\tilde{\lambda}_0 \equiv \mu \lambda_0$ the dimensionless angular eigenvalue, and λ_0 and S_0 the leading-order value and form of λ and S . The solutions are the associated Legendre polynomials P_{jm} , if the separation constant satisfies $\tilde{\lambda}_0(\tilde{\lambda}_0 - 1) = j(j + 1)$, so it has two solutions $\tilde{\lambda}_0^+ = -j$ and $\tilde{\lambda}_0^- = j + 1$.

By substituting the explicit expressions of $B^{\mu\nu}$ in the leading form of the separable ansatz, and taking the large distance limit $r \gg \lambda_0$, the spatial components of the vector field simplify to [42]

$$A_0^i \propto r^{-1} R_0^{\text{far}}(r) (r \partial^i Y_{jm} - \lambda_0 Y_{jm} \hat{r}^i) e^{-i\omega t}, \quad (33)$$

where Y_{jm} are the scalar spherical harmonics, they relate to the electric vectorial spherical harmonics $Y_{j\pm 1, jm}^i$ via

$$\begin{cases} Y_{j-1, jm}^i = \frac{1}{\sqrt{j(2j+1)}} [r \partial^i Y_{jm} + j Y_{jm} \hat{r}^i] \\ Y_{j+1, jm}^i = \frac{1}{\sqrt{(j+1)(2j+1)}} [r \partial^i Y_{jm} - (j+1) Y_{jm} \hat{r}^i], \end{cases} \quad (34)$$

by observing and matching the coefficients in front of Y_{jm} , we identify $\tilde{\lambda}_0^\pm$ correspond to the $j = l \pm 1$ electric modes respectively. Up to this point, the explicit expression of $R_0^{\text{far}}(r)$ is not shown, it should be given by matching different pieces of asymptotic expansions and fixing the boundary conditions, which we will do in the next subsections.

C. Matching three pieces of asymptotic expansions in the radial function

In this subsection, we take into account the complete radial range that extends from the BH outer horizon r_+ to spatial infinity in the electric modes, by the method of matched asymptotic expansion. But as mentioned earlier, the additional poles gave rise to the necessity to introduce an intermediate region to match near and far pieces, to obtain the full range behavior.

By defining a rescaled radial coordinate as $x \equiv 2\sqrt{\mu^2 - \omega^2}(r - r_+)$, which mapped the nearer regions to $x \sim \alpha^2$ and the Bohr radius $r_c \sim \alpha^{-1}$ to $x \sim 1$, the differential equation in this coordinate reads,

$$\left[\frac{d^2}{dx^2} + \frac{\nu_0}{x} - \frac{\lambda_0(\lambda_0 + 1)}{x^2} - \frac{1}{4} \right] R_0^{\text{far}} = 0 \quad (35)$$

with ν_0 the leading order of $\nu \equiv M\mu^2/\sqrt{\mu^2 - \omega^2}$, defined in (21); the solutions are given as

$$R_{\text{far}}(x) = e^{-x/2} x^{l+1} U(l+1-\nu_0, 2+2l, x), \quad (36)$$

with $U(\dots)$ the confluent hypergeometric function of the second kind; for integer values of $\nu_0 \geq l+1$, it becomes the Laguerre polynomials appearing in the non-relativistic solution (18), which once more suggests the hydrogenic features. Here we omitted possible coefficient in the solution, which is ready to be eliminated by matching to other pieces in the procedure.

For the region near the outer horizon, we define the rescaled coordinate $z \equiv (r - r_+)/ (r_+ - r_-)$, representing distance from the outer horizon in unit of $(r_+ - r_-)$, and mapping the inner, outer horizon and spatial infinity to $z = -1, 0, \infty$. In Eq. (29), we can ignore the terms that contain $(r - \hat{r}_\pm)$ in the denominator and identify A_\pm as $2P_+^2$ in the small α approximation. Hence the leading-order radial equation of the near region is

$$\left[\frac{d^2}{dz^2} + \left(\frac{1}{z} + \frac{1}{z+1} \right) \frac{d}{dz} - \frac{j(j+1)}{z(z+1)} + \frac{P_+^2}{z^2} + \frac{P_+^2}{(z+1)^2} - \frac{2P_+^2}{z} + \frac{2P_+^2}{z+1} \right] R_0^{\text{near}} = 0, \quad (37)$$

the corresponding solutions are known as Kummer's solutions, with three pairs of equivalent basis denoted by $\{w_1, w_2\}, \{w_3, w_4\}, \{w_5, w_6\}$ near the poles at $z = -1, 0, \infty$ respectively. With physically acceptable purely outgoing solutions at the inner horizon, w_1 is used in [42], while the choice of $\{w_5, w_6\}$ is adopted in [96] to match solutions with far region in scalar case; however, in our vector case here, equation (37) only holds in the near region hence is no longer valid as $z \rightarrow \infty$, and further to better match the boundary condition with reflection near the outer horizon, we identify $\{w_3, w_4\}$ as the proper basis, which is our optimization to the matching procedure, saving from switching between different pairs of basis employed in [96]; in this regard, the solution reads

$$R_0^{\text{near}}(z) = \left(\frac{z}{z+1} \right)^{iP_+} [C_0^{\text{near}} w_3(z) + D_0^{\text{near}} w_4(z)], \quad (38)$$

with

$$\begin{cases} w_3(z) \equiv {}_2F_1(-j, j+1, 1+2iP_+, -z), \\ w_4(z) \equiv (-z)^{-2iP_+} {}_2F_1(-j-2iP_+, j+1-2iP_+, 1-2iP_+, -z), \end{cases} \quad (39)$$

where we have changed the argument $z \rightarrow -z$ to express the basis in terms of hypergeometric function ${}_2F_1(\dots)$.

In order to obtain the full-range radial solution, one must try to extend the near and far region towards each other, which should be achieved by taking the limits $x \rightarrow 0$ and $z \rightarrow +\infty$ respectively;

However, as we've mentioned, the existence of the poles $r = \hat{r}_\pm$ of the radial equation (29) fails to join the two regions, leading to the necessity in introduce an intermediate region, which is expressed by defining a rescaled radial coordinate $y \equiv \mu(r - r_+)$; the equation for the intermediate region is then [42]

$$\left[\frac{d^2}{dy^2} + \left(\frac{2}{y} - \frac{2y}{\tilde{\lambda}_0^2 + y^2} \right) \frac{d}{dy} - \frac{\tilde{\lambda}_0(\tilde{\lambda}_0 - 1)}{y^2} - \frac{2\tilde{\lambda}_0}{\tilde{\lambda}_0^2 + y^2} \right] R_0^{\text{int}} = 0, \quad (40)$$

which has the corresponding solution

$$R_0^{\text{int}}(y) = C_0^{\text{int}} y^{-\tilde{\lambda}_0} + D_0^{\text{int}} y^{-1+\tilde{\lambda}_0} \left[\tilde{\lambda}_0^2 (2\tilde{\lambda}_0 + 1) + (2\tilde{\lambda}_0 - 1) y^2 \right], \quad (41)$$

with power indices in polynomials determined by the angular eigenvalues $\tilde{\lambda}_0(\tilde{\lambda}_0 - 1) = j(j + 1)$, as the same in (32). Since the calculation for the two eigenvalues are parallel, here we only take $\tilde{\lambda}_0 = \tilde{\lambda}_0^+ = -j = -(l + 1)$ in the following procedure and directly present results for $\tilde{\lambda}_0 = \tilde{\lambda}_0^- = j + 1 = l$.

To match the three pieces of asymptotic solutions (36)(38)(40) in two overlap regions, new matching coordinates should be defined [42],

$$\begin{cases} \xi_1 \equiv \frac{x}{\alpha^\beta} = \frac{2}{\nu} \frac{y}{\alpha^{\beta-1}}, & 0 < \beta < 1, \\ \xi_2 \equiv \frac{2\mu(r_+ - r_-)}{\nu} \frac{z}{\alpha^{\beta-1}} = \frac{2}{\nu} \frac{y}{\alpha^{\beta-1}}, & 1 < \beta < 2, \end{cases} \quad (42)$$

with ξ_1 connecting x and y , and ξ_2 connecting z and y . In these new coordinates, by keeping the leading order in α -expansions and taking the relevant limits of radial coordinates, the behaviors of the near, intermediate and far solutions are given as

$$\begin{aligned} R_0^{\text{near}} \sim & C_0^{\text{near}} \left[2^{-j} \left(\frac{\alpha^{\beta-1}\nu}{\mu(r_+ - r_-)} \right)^j \xi_2^j - 2^{1+j} \left(\frac{\alpha^{\beta-1}\nu}{\mu(r_+ - r_-)} \right)^{-j-1} \xi_2^{-j-1} \mathcal{I}_j \right] \\ & + D_0^{\text{near}} \left[2^{-j} \left(\frac{\alpha^{\beta-1}\nu}{\mu(r_+ - r_-)} \right)^j \xi_2^j + 2^{1+j} \left(\frac{\alpha^{\beta-1}\nu}{\mu(r_+ - r_-)} \right)^{-j-1} \xi_2^{-j-1} \mathcal{I}_j \right]; \end{aligned} \quad (43)$$

$$\begin{cases} R_0^{\text{int}} \sim C_{\text{int}} 2^{-j} (\alpha^{\beta-1}\nu)^j \xi_2^j - D_{\text{int}} 2^{j+1} j^2 (2j - 1) (\alpha^{\beta-1}\nu)^{-j-1} \xi_2^{-j-1}, \end{cases} \quad (44)$$

$$\begin{cases} R_0^{\text{int}} \sim C_{\text{int}} 2^{-j} (\alpha^{\beta-1}\nu)^j \xi_1^j - D_{\text{int}} 2^{j-1} (2j + 1) (\alpha^{\beta-1}\nu)^{1-j} \xi_1^{1-j}; \end{cases} \quad (45)$$

$$\begin{aligned} R_0^{\text{far}} \sim & \frac{\Gamma(2j - 1)}{\Gamma(-\nu)} (\alpha^\beta \xi_1)^{1-j} + \frac{\Gamma(1 - 2j)}{\Gamma(1 - 2j - \nu)} (\alpha^\beta \xi_1)^j \\ \sim & (-1)^{n+1} \delta\nu (2j - 2)! n! (\alpha^\beta \xi_1)^{1-j} + (-1)^n \frac{(n + 2j - 1)!}{(2j - 1)!} (\alpha^\beta \xi_1)^j. \end{aligned} \quad (46)$$

where in (43) coefficients are, for convenience, rescaled as $\mathcal{C}_0^{\text{near}} \equiv C_0^{\text{near}} \Gamma(1 + 2iP_+)$ and $\mathcal{D}_0^{\text{near}} \equiv D_0^{\text{near}} \Gamma(1 - 2iP_+) e^{2P_+\pi}$, and we used the notation

$$\mathcal{I}_j \equiv \frac{(j!)^2}{(2j)!(2j+1)!} i^{P_+} \prod_{q=1}^j (q^2 + 4P_+^2), \quad (47)$$

which is purely imaginary. Approximations of Gamma functions around negative integer arguments in (46) are taken to be the leading terms in Laurent expansions $\Gamma(-n + \epsilon) \sim (-1)^n / (n! \epsilon)$ with n a positive integer and ϵ an infinitesimal quantity; we see that $\delta\nu$ only appears in the coefficient of the first term, but is suppressed in the ratio of two infinities in the second.

Matching between near and intermediate region goes straightforward by comparing coefficients of ξ^j and ξ^{-j-1} in (43) and (44), we obtain

$$\begin{cases} C_{\text{int}} = (\mathcal{C}_0^{\text{near}} + \mathcal{D}_0^{\text{near}}) \mu^{-j} (r_+ - r_-)^{-j}, \\ D_{\text{int}} = (\mathcal{C}_0^{\text{near}} - \mathcal{D}_0^{\text{near}}) \mu^{j+1} (r_+ - r_-)^{j+1} \frac{\mathcal{I}_j}{j^2 (2j-1)}, \end{cases} \quad (48)$$

and the parallel process to match the intermediate and far regions results in

$$\begin{cases} C_{\text{int}} = (2k)^j \mu^{-j} \frac{(n+2j-1)!}{(2j-1)!}, \\ D_{\text{int}} = -(2k)^{1-j} \mu^{j-1} \delta\nu (2j-2)! n!. \end{cases} \quad (49)$$

with $k \equiv \sqrt{\mu^2 - \omega^2}$ defined for simplicity. Joining (48) and (49), coefficients in the intermediate region are dropped, and we get relation between the energy level correction $\delta\nu$ and coefficients in the near region as

$$\delta\nu = \frac{\mathcal{C}_0^{\text{near}} - \mathcal{D}_0^{\text{near}}}{\mathcal{C}_0^{\text{near}} + \mathcal{D}_0^{\text{near}}} (2k)^{2j-1} (r_+ - r_-)^{2j+1} \mu^2 \frac{(2j+1)}{[j(2j-1)!]^2} \frac{(n+2j-1)!}{n!} \mathcal{I}_j, \quad (50)$$

which holds only for $j = l + 1$ as we stated above. For $j = l - 1$, the result is given by the similar process as

$$\delta\nu = \frac{\mathcal{C}_0^{\text{near}} - \mathcal{D}_0^{\text{near}}}{\mathcal{C}_0^{\text{near}} + \mathcal{D}_0^{\text{near}}} (2k)^{2j+3} (r_+ - r_-)^{2j+1} \mu^{-2} \frac{(j+1)^2}{(2j+1)[(2j+2)!]^2} \frac{(n+2j+3)!}{n!} \mathcal{I}_j. \quad (51)$$

These two equations can be consolidated into a unified form for $j = l \pm 1$ that reads

$$\delta\nu = \frac{\mathcal{C}_0^{\text{near}} - \mathcal{D}_0^{\text{near}}}{\mathcal{C}_0^{\text{near}} + \mathcal{D}_0^{\text{near}}} (2k)^{2l+1} (r_+ - r_-)^{2j+1} \mu^{2(j-l)} \frac{(2j)!(2j+1)!(l!)^2}{[j!(j+l)!(j+l+1)!]^2} \frac{(n+2l+1)!}{n!} \mathcal{I}_j. \quad (52)$$

Thus the energy level correction $\delta\nu$ is solely determined by the coefficients in near region, which is further to be identified by the boundary condition at the outer horizon, that we will introduce in the next section.

III. THE CORRECTED SPECTRUMS WITH NEAR-HORIZON REFLECTION AND SUPERRADIANT GROWTH ANOMALY

A. Reflective boundary conditions near the horizon and corrected superradiance rate

Classically, considering the asymptotic behavior of the near radial function, the purely-ingoing boundary conditions at BH horizons follows from the regularity requirements [104] as

$$\lim_{r_* \rightarrow -\infty} R(r_*) \sim e^{-i(\omega - m\Omega_{\pm})r_*}. \quad (53)$$

with the tortoise coordinate r_* defined as

$$r_* = r + \frac{2Mr_+}{r_+ - r_-} \ln \frac{r - r_+}{2M} - \frac{2Mr_-}{r_+ - r_-} \ln \frac{r - r_-}{2M}, \quad (54)$$

where Ω_{\pm} are chosen at $r \rightarrow r_{\pm}$ respectively and $\Omega_+ \equiv \Omega_H$. In terms of the coordinate z , one can check that in the near region, the purely ingoing conditions are equivalent to $\lim_{z \rightarrow 0} R(z) \sim z^{iP_+}$ and $\lim_{z \rightarrow -1} R(z) \sim (z+1)^{-iP_+}$, hence $R^{\text{near}}(z) \sim (\frac{z}{z+1})^{iP_+}$, consistent with equation (38) with a vanishing $D^{\text{near}}w_4(z)$ term; the existence of $w_4(z)$ imposes an outgoing term at the outer horizon via $z^{iP_+} \rightarrow z^{-iP_+}$, while keeps the ingoing condition at the inner horizon fixed.

Coincidentally, one of the possible consequences of potential microstructures of the horizon, e.g., area quantization [88, 89], would phenomenologically introduce a reflection parameter \mathcal{R} at the horizon, to encode the modification to a classical BH by including an outgoing term in the boundary condition as

$$\lim_{r \rightarrow r_+} R(r_*) \sim e^{-i(\omega - m\Omega_H)r_*} + \mathcal{R}(\omega) e^{i(\omega - m\Omega_H)r_*}, \quad (55)$$

which effectively, in terms of coordinate z , utilize the basis $w_4(z) \sim z^{-iP_+}$ in the near region solution $R^{\text{near}}(z)$. Note that we always keep the superradiance term $(\omega - m\Omega_H)$ in front of the coordinates, since from the ansatz (25), we have $e^{-i\omega t} e^{im\phi} R(r_*) = e^{-i(\omega - m\Omega_H)t} R(r_*)$ at the horizon, so this form guarantees the solutions *physically* ingoing/outgoing in addition to observed in coordinates [105]. And here we once again emphasize the significance of the quantity P_+ , with its positivity/negativity denoting a state superradiant or absorptive, while the signs in front denoting a boundary condition ingoing or outgoing; we summarize and list it in Table II for clarity, within which the colored text in left-bottom grid is what we consider in the context.

We further assume $\mathcal{R}(\omega)$ to be real for elegancy, different from that in [96] by a phase factor; the spectrum of $\mathcal{R}(\omega)$ is determined from quantum gravity [88]. The boundary condition (55) is to be

	$P_+ > 0$	$P_+ < 0$
z^{iP_+} term only	superradiance & (purely ingong) B.C.	absorption & (purely ingong) B.C.
z^{-iP_+} term added	superradiance & (ingong + outgoing) B.C.	absorption & (ingong + outgoing) B.C.

TABLE II. States & boundary conditions (B.C.) in terms of P_+ . $P_+ > 0$ or $P_+ < 0$ denotes superradiance or absorption state; B.C. containing z^{iP_+} term only or additional z^{-iP_+} term denotes purely ingong or outgoing included flow of the field.

compared with near region solution (38), which is manifestly a linear combination of an ingong and an outgoing term, weighted by C_0^{near} and D_0^{near} respectively. The reflection parameter then can be extracted by taking the ratio of the coefficients $\mathcal{R} = D_0^{\text{near}}/C_0^{\text{near}} = \mathcal{D}_0^{\text{near}}/\mathcal{C}_0^{\text{near}} [\Gamma(1 - 2iP_+)e^{2P_+\pi}/\Gamma(1 + 2iP_+)]$, which is brought into (52) to obtain the form of (24) as

$$\delta\nu = \delta\bar{\nu} \frac{1 - \mathcal{R} \exp\left(2i \sum_{q=1}^j \phi_q\right)}{1 + \mathcal{R} \exp\left(2i \sum_{q=1}^j \phi_q\right)}, \quad \text{with} \quad \phi_q \equiv \arctan \frac{2P_+}{q}, \quad (56)$$

which shares the same form as that in the scalar field case [96], but with the orbital angular momentum l replaced by the total angular momentum j . It is straightforward to identify the reflection correction defined in (24) as

$$\Phi(\mathcal{R}) = \frac{1 - \mathcal{R} e^{i\phi_w}}{1 + \mathcal{R} e^{i\phi_w}} = \frac{1 - \mathcal{R}^2 - 2i\mathcal{R} \sin \phi_w}{1 + \mathcal{R}^2 + 2\mathcal{R} \cos \phi_w}, \quad \text{with} \quad \phi_w = 2 \sum_{q=1}^j \phi_q. \quad (57)$$

By setting $\mathcal{R} = 0$, we obtain the energy shifts $\delta\bar{\nu}$ without reflection, which can be directly read out from (52) by dropping relevant coefficients, and is observed to be a purely imaginary number in the presence of \mathcal{I}_j . Now that we already have $\delta\nu$ in hand, according to (22), we can immediately get $\delta\omega$ as

$$\begin{cases} \text{Re}(\delta\omega) = i\delta\bar{\nu} \frac{M^2\mu^3}{\bar{n}^3} \text{Im}[\Phi(\mathcal{R})] = -i\delta\bar{\nu} \frac{M^2\mu^3}{\bar{n}^3} \frac{2\mathcal{R} \sin \phi_w}{1 + \mathcal{R}^2 + 2\mathcal{R} \cos \phi_w} \\ \text{Im}(\delta\omega) = -i\delta\bar{\nu} \frac{M^2\mu^3}{\bar{n}^3} \text{Re}[\Phi(\mathcal{R})] = -i\delta\bar{\nu} \frac{M^2\mu^3}{\bar{n}^3} \frac{1 - \mathcal{R}^2}{1 + \mathcal{R}^2 + 2\mathcal{R} \cos \phi_w}. \end{cases} \quad (58)$$

According to (23), the imaginary part $\text{Im}(\delta\omega)$ directly contributes to superradiant rate Γ , while the real part $\text{Re}(\delta\omega)$ is to be compared with ω_0 ; since ω_0 is expanded by orders of $\alpha = M\mu$, we extract powers of M and ν in (52) as, $k = \sqrt{\mu^2 - \omega^2} \sim \mu\alpha$, $r_+ - r_- = 2\sqrt{M^2 - a^2} \sim M$ and $P_+ \sim \alpha$, so together we have $-i\delta\bar{\nu} M^2\mu^3/\bar{n}^3 \propto (M\mu)^{2l+2j+3} M^2\mu^3 = \mu(M\mu)^{2l+2j+5} < \mu(M\mu)^5$ when $j \geq 1$. Now that energy levels expanded to α^5 is already known [42], we can safely use the result by omitting the shift caused by reflection, which is

$$E_{\bar{n}ljm} = \mu \left(1 - \frac{\alpha^2}{2\bar{n}^2} - \frac{\alpha^4}{8\bar{n}^4} + \frac{f_{\bar{n}lj}}{\bar{n}^3} \alpha^4 + \frac{h_{lj}}{\bar{n}^3} \chi m \alpha^5 + \dots \right), \quad (59)$$

with

$$\begin{cases} f_{\bar{n}lj} = -\frac{4(6lj + 3l + 3j + 2)}{(l+j)(l+j+1)(l+j+2)} + \frac{2}{\bar{n}} \\ h_{lj} = \frac{16}{(l+j)(l+j+1)(l+j+2)}. \end{cases} \quad (60)$$

The superradiance rate with reflection is given as

$$\Gamma_{\bar{n}jlm} = \bar{\Gamma}_{\bar{n}jlm} \text{Re}[\Phi(\mathcal{R})] \quad (61)$$

with $\bar{\Gamma}_{\bar{n}jlm}$ the rate without reflection,

$$\begin{aligned} \bar{\Gamma}_{\bar{n}jlm} = -i\delta\bar{\nu} \frac{M^2\mu^3}{\bar{n}^3} &= \frac{(r_+ - r_-)^{2j+1}}{M^{2j+2}} \alpha^{2l+2j+5} (-i\mathcal{I}_j) \\ &\times \frac{2^{2l+2j-2} (\bar{n} + l + 1)!}{(\bar{n} - l - 1)^{2l+4} \bar{n}!} \frac{(2j)! (2j+1)! (l!)^2}{[j! (j+l)! (j+l+1)!]^2} \left[1 + \frac{2(1+l-j)(1-l+j)}{l+j} \right], \end{aligned} \quad (62)$$

where the last term in the square brackets is also the best educated guess in Ref. [42] for the magnetic modes ($l = j$), so we write it for completeness of the results.

In this work, we focus on the fastest growing mode in the electric mode, i.e., $\{\bar{n}, l, j, m\} = \{1, 0, 1, 1\}$, with vanishing cloud angular momentum; since in this mode, the BH spin is totally transferred to the intrinsic spin of the vector field, as we've mentioned in the introduction, making the possible signals most sensitive to the near-horizon geometry of the BH. Here we study the effect of the reflection parameter \mathcal{R} on the dominant superradiant growth rate Γ_{1011} in terms of the mass coupling $\alpha = M\mu$, with different values of BH spin χ , as illustrated in Fig. II. We divide the figure into left and right part: in the left part we plot curves with more values of \mathcal{R} to observe the change of the superradiant rate as the reflection parameter varies; in the right part we only plot curves with a zero and a non-zero reflection parameter, but with additional numerical results. The numerical results are obtained using the direct integration method, which is introduced in Ref. [58], but here we use the boundary condition (55) adjusted for reflection. It is seen that the numerical data points lie above the analytical curves, due to the fact that analytical calculations are performed to leading order only, whereas numerical results are computed using the complete expression. It is evident from the comparison that the analytical results are more applicable for cases with small coupling, which is the focus of this study.

We observe that in the left part, generally the system with a greater reflection parameter has a lower superradiance rate, as shown in the middle and bottom panels; however, an anomalous behavior emerges when the BH spin is high enough (e.g., $\chi = 0.99$) and the mass coupling is small, as depicted in the top panel: an initial increase in the superradiance rate occurs as the reflection parameter rises, then followed by a decrease, which is marked out in the purple dashed box.

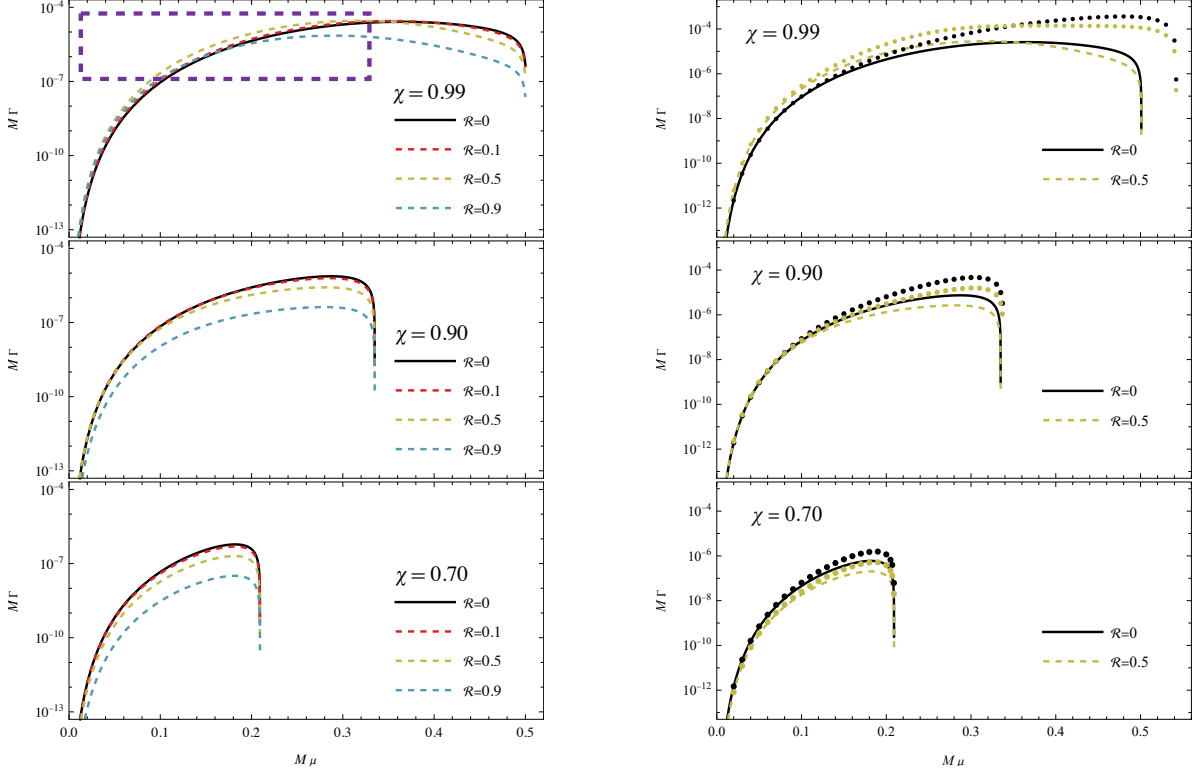


FIG. II. Analytic asymptotic (solid and dashed lines) and numerical (dotted lines) results of the dominant superradiant growth rate Γ_{1011} as a function of the mass coupling $\alpha = M\mu$. The BH angular momentum χ varies: 0.99, 0.9, 0.7 (from top to bottom). The black solid curve denotes cases without reflection. The colored dashed curves (left) and the yellow dotted curves (right) label different reflection parameters \mathcal{R} , with the analytic approximation given by Eqs. (61) and (62). The purple dashed box in the left figure marks out the rough region where the anomalous situation occurs: the superradiance rate is initially increased and then decreased when \mathcal{R} becomes larger and larger, when the mass coupling is small and BH spin is as high as $\chi = 0.99$.

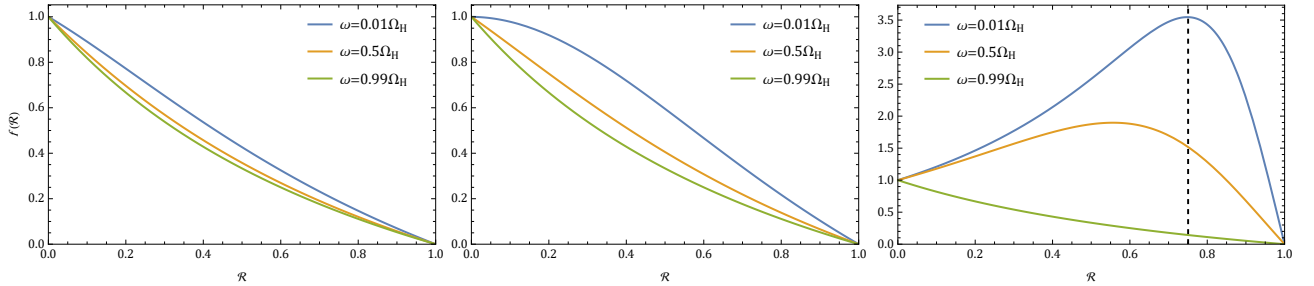


FIG. III. The superradiance modifier $f(\mathcal{R})$ as a function of the reflection parameter \mathcal{R} for various (χ, ω) values: the BH spin $\chi = 0.5$, $\chi = 1/\sqrt{2}$, and $\chi = 0.99$ cases are shown respectively in left, middle, and right panels, with $\omega = 0.01\Omega_H$ (in blue), $\omega = 0.5\Omega_H$ (in orange), and $\omega = 0.99\Omega_H$ (in green). In the right panel, the critical reflection $\mathcal{R}_c \simeq 0.75$ supporting the highest value of $f(\mathcal{R}_c) \simeq 3.5$ is labeled by the dashed vertical line.

B. The superradiance modifier and the growth anomaly conditions

To mathematically investigate this temporary anomalous situation, we extract the “superradiance modifier” from Eq. (61) as

$$f(\mathcal{R}) \equiv \Gamma_{1011}/\bar{\Gamma}_{1011} = \text{Re}[\Phi(\mathcal{R})]_{j=1} = \frac{1 - \mathcal{R}^2}{1 + \mathcal{R}^2 + 2\mathcal{R} \cos(2\phi_1)}, \quad (63)$$

with $\phi_1 = \arctan(2P_+)$. Observe that with the increase of \mathcal{R} , there is a competition between the numerator and the denominator, which is judged by the magnitude of $-\mathcal{R}$ and $\cos(2\phi_1)$; the anomalous situation occurs when the denominator goes down faster, i.e.,

$$-\mathcal{R} > \cos[2 \arctan(2P_+)] = \frac{2}{1 + (2P_+)^2} - 1, \quad (64)$$

and here in case of $m = 1$, we use the form of (31) to give

$$2P_+ = \underbrace{\frac{\chi}{\sqrt{1 - \chi^2}} \left(1 - \frac{\omega}{\Omega_H}\right)}_{\text{anomalous growth condition}} > \sqrt{\frac{1 + \mathcal{R}}{1 - \mathcal{R}}} \geq 1, \quad (65)$$

where the underlined inequality is just the anomalous growth condition. We see that both the BH spin χ and the superradiance saturation ω/Ω_H play roles here.

Firstly and roughly, given that $1 - \omega/\Omega_H < 1$, to make $2P_+ > 1$, the BH spin χ should be at least greater than $1/\sqrt{2}$, otherwise no anomaly can happen, let alone in the presence of increasing ω/Ω_H and non-zero \mathcal{R} , the BH spin χ should be even larger, that's why we've only observed the anomaly in the left top panel of Fig. II; the critical spin χ^c that anomaly can happen generally depends on the two parameters $\chi^c(\omega/\Omega_H, \mathcal{R})$, with the special case $\chi^c(\omega/\Omega_H \rightarrow 0, \mathcal{R} \rightarrow 0) = 1/\sqrt{2}$ consistent with that we've mentioned. Later as the system evolves, the superradiance saturation ω/Ω_H goes up and the spin χ goes down, making the inequality (65) invalid again at some point. Secondly, given the BH spin, there's a constraint on the mass coupling α , by writing the saturation as $\omega/\Omega \simeq 2\alpha(1 + \sqrt{1 - \chi^2})/\chi$, we see that if $\alpha < \alpha_\chi \equiv (\chi - \sqrt{1 - \chi^2})/[2(1 + \sqrt{1 - \chi^2})]$, it would lead to $2P_+ < 1$, making the anomaly invalid. In high spin case, $\alpha \in (\alpha_{\chi=1/\sqrt{2}}, \alpha_{\chi=1}) = (0, 0.5)$, there's no anomaly in high mass coupling greater than a half. In particular, for the top panels in Fig. II, $\alpha_{\chi=0.99} \simeq 0.37$, it is roughly the turning point for $f(\mathcal{R} = 0.5) \simeq f(\mathcal{R} = 0)$. To summarize, there are two ingredients necessary to the anomaly: (1) an initial extremely high spin BH; (2) the superradiance is in the low saturation state. Along with that, the turning point \mathcal{R}_c where the modifier terminates its boost is calculated by setting $f'(\mathcal{R}) = 0$ and $f''(\mathcal{R}) < 0$, we get

$$\mathcal{R}_c = \frac{\sin(2\phi_1) - 1}{\cos(2\phi_1)} = \frac{\tan \phi_1 - 1}{\tan \phi_1 + 1} = \frac{2P_+ - 1}{2P_+ + 1} = 1 - \frac{2}{1 + 2P_+}, \quad (66)$$

which is specified when χ and ω/Ω_H is given. Numerical values of turning points are shown in Fig. III, e.g., we use black dashed line to highlight the case where $\mathcal{R}_c \simeq 0.75$ when $\chi = 0.99$ and $\omega/\Omega_H = 0.01$. It is noted that both the high spin and the low saturation are necessary to guarantee the existence and positivity of \mathcal{R}_c .

More elegant geometric forms of the anomaly condition (65) can be obtained, by parametrizing the reflection parameter as $\mathcal{R} \equiv \cos(2\phi_{\mathcal{R}})$ with $\phi_{\mathcal{R}} \in [0, \pi/4]$, hence $\sqrt{(1+\mathcal{R})/(1-\mathcal{R})} = \cot \phi_{\mathcal{R}}$, and recalling $2P_+ = \tan(\phi_1)$, we have

$$\tan \phi_1 \tan \phi_{\mathcal{R}} > 1. \quad (67)$$

This can also be achieved by viewing the modifier as square of a ratio between two length,

$$f(\mathcal{R}) = \frac{1 + \mathcal{R}^2 - 2\mathcal{R} \cos(2\phi_{\mathcal{R}})}{1 + \mathcal{R}^2 - 2\mathcal{R} \cos(\pi - 2\phi_1)} \equiv \frac{\mathcal{T}^2}{\mathcal{L}^2}, \quad (68)$$

with $\mathcal{T} = \sin(2\phi_{\mathcal{R}}) = \sqrt{1 - \mathcal{R}^2}$ the transmission rate at the boundary, and \mathcal{L} some kind of a side length of a triangle with other two side lengths 1 and \mathcal{R} , and an angel $\pi - 2\phi_1$ between them. The anomaly holds when $\mathcal{T} > \mathcal{L}$, i.e., $2\phi_{\mathcal{R}} > \pi - 2\phi_1$, or simply

$$\phi_{\mathcal{R}} + \phi_1 > \frac{\pi}{2}, \quad (69)$$

which is equivalent to equation (67). The geometric forms (67) and (69) leads us to a pictorial description of the anomalous growth as shown in Fig. IV: The pointers $\vec{\mathcal{R}}$ and $\vec{\phi}_1$ are “the reflection state” and “the superradiance state” denoted by arrows pointing at half a unit circle above the horizontal axis, with the former deviated from the positive x -axis by the angle $2\phi_{\mathcal{R}}$, and the later from the negative x -axis by the angle $2\phi_1$; the projection of $\vec{\mathcal{R}}$ onto the x -axis is the reflection paramter \mathcal{R} chosen to be ranged from 0 to 1; the sides \mathcal{T} and \mathcal{L} connect endpoints of $\vec{\mathcal{R}}$ and $\vec{\phi}_1$ to the point where the value of \mathcal{R} locates. Hence, $\vec{\mathcal{R}}$ is restricted in the first quadrant and $\vec{\phi}_1$ is allowed to slide counter-clockwise in the whole upper plane. If the initial superradiance state $\vec{\phi}_1$ is located on the left of the reflection state $\vec{\mathcal{R}}$, no anomaly happens; on the contrary, if $\vec{\phi}_1$ is located on the right of $\vec{\mathcal{R}}$, anomaly happens in the region where blue and red arcs overlap and then vanishes when $\vec{\phi}_1$ evolves and slides passing through $\vec{\mathcal{R}}$.

Furthermore, by observing the form of (31) and (2), we find

$$2P_+ = \frac{m\Omega - \omega}{\kappa_+} = -\frac{\omega}{8\pi} \frac{\delta A}{\delta M} = \frac{1}{2\pi k_B} \frac{\delta S_{\text{BH}}}{\delta N}, \quad (70)$$

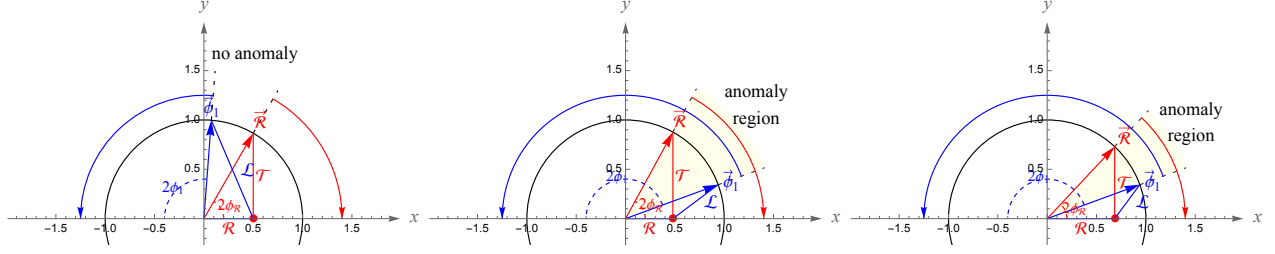


FIG. IV. Geometrical presentation of cases with different reflection state and superradiance state, denoted by red and blue pointers $\vec{\mathcal{R}}$ and $\vec{\phi}_1$ respectively, with the former chosen to be located in the first quadrant while the later sliding dynamically from the first to second quadrant, the corresponding ranges are denoted by red and blue arcs outside the unit circle. The angle $2\phi_{\mathcal{R}}$ is between $\vec{\mathcal{R}}$ and the positive x -axis, while $2\phi_1$ is between $\vec{\phi}_1$ and the negative x -axis. The sides \mathcal{T} and \mathcal{R} are sides facing to $2\phi_{\mathcal{R}}$ and $\pi - 2\phi_1$ respectively. The left and the middle figures share the same reflection state $\vec{\mathcal{R}}$, but with different initial superradiance state $\vec{\phi}_1$; the middle and the right figures share the same different initial superradiance state $\vec{\phi}_1$, but with different reflection state $\vec{\mathcal{R}}$. The anomaly happens when $2\phi_{\mathcal{R}} + 2\phi_1 > \pi$ (or $\mathcal{T} > \mathcal{L}$), and vanishes when $2\phi_{\mathcal{R}} + 2\phi_1 < \pi$ (or $\mathcal{T} < \mathcal{L}$).

with the surface gravity $\kappa_+ = (r_+ - r_-)/4Mr_+$ and $\delta N = \delta M_c/\omega = -\delta M/\omega$ the growth of boson occupation number, and further we used the BH entropy $S_{\text{BH}} = k_B A/4$. In a quasi-adiabatic system containing roughly only the BH and bosonic condensate, $\delta S_{\text{BH}} = -\delta S_c = \delta I$, with $I = -S_c$ the information carried away by bosonic condensates, the anomaly condition can be expressed as

$$\frac{\delta I}{\delta N} > 2\pi k_B \cot \phi_{\mathcal{R}}, \quad (71)$$

which states that growth anomaly happens when information per particle carries exceeds a certain value determined by the reflection parameter. This is more profound than the geometric expressions (69)(67), and may reveal some relations between this anomaly and BH information and microscopic structure. Equation (71) serve as our most concise expression for the anomaly condition, with physics behind \mathcal{R} yet to be implemented in the future work.

We should mention that in spite of different expressions, the anomaly conditions are manifestations of “rotation-relativistic” effect of a cold ($\chi \simeq 1$) or at most warm ($\chi \gtrsim 1/\sqrt{2} \simeq 0.7$) BH^2 , whose rotational energy is leading to or at least comparable to the mass energy, which is analogous to the difference of the kinetic energy $m_0 c^2 [(1 - v^2/c^2)^{-1/2} - 1]$ and the rest energy $m_0 c^2$ in special relativity [1]. The energy stored in spin is a very sensitive function of the spin parameter χ , superradiance turns

² Note that “hot” and “cold” BHs are defined from the temperature in BH thermodynamics, which are reverse to the concepts of “hot” and “cold” particles by moving velocity.

a BH from a relativistic/cold to a non-relativistic/hot one. Possible hints and clearer physics by these expressions deserves further explorations and investigations.

IV. EFFECTS OF REFLECTION ON THE BH-CONDENSATE EVOLUTION AND ANOMALY FEATURES

In this section, we explore the effects of the reflection parameter on the evolution of the BH-condensate system and particularly focus on the case where the anomalous enhancement of superradiant growth is obvious. We provide an overview of the general evolution in Subsection IV A, and then focus on the characteristic quantities of the growth anomaly and the induced GW strain deformation in Subsection IV B.

A. General evolutions and final state estimates

In general, the evolution of the BH-condensate system consists of the following two ingredients: the exchange of energy and angular momentum between the BH and the contents outside the horizon, the loss of energy and angular momentum of the system due to GW emissions via annihilation or level transition in the condensates, see equation (20); we will neglect the transition channel in the following analysis since we focus on the single vector dominant mode $\{\bar{n}, l, j, m\} = \{1, 0, 1, 1\}$ only. We will also ignore effects of matter accretion and GWs falling towards the horizon in this study.

In this regard, the system is closed by the energy and angular momentum conservation:

$$\begin{cases} \dot{M} + \dot{M}_v = -\dot{E}_{\text{GW}}, \\ \dot{J} + \dot{J}_v = -\dot{J}_{\text{GW}}. \end{cases} \quad (72)$$

with M_v and J_v the total mass and angular momentum of the vectorial condensate. The ratio between changes of angular momentum and mass per unit time of the condensates and GWs are just the same as that of a particle [106],

$$\frac{\dot{J}_v}{\dot{M}_v} = \frac{\dot{J}_{\text{GW}}}{\dot{E}_{\text{GW}}} = \frac{m}{\omega}, \quad (73)$$

straightforward as it is, condensates and GWs are due to growth and decays of these particles.

The growth of the condensates obey

$$\dot{M}_v = 2\Gamma M_v - \Gamma_{\text{ann}} M_v^2, \quad (74)$$

where the superradiant rate Γ is defined through equation (23) denoting the changing rate of the field amplitude, and the factor of 2 comes from the fact that the condensate mass should be relevant to the changing rate of the energy density (or occupation number) [54]; Γ_{ann} is the annihilation rate within the single energy level $\bar{n} = 1$, which is much smaller than the typical values of superradiance rate [64].

If the initial condition satisfies $\omega < m\Omega_{\text{H}}$, the condensate will endure an exponential growth in the superadiant stage, until the saturation when the condensate mass reaches its maximum:

$$M_{\text{v}}^{\text{max}} \approx M_{\text{v}}^0 \exp \left[\int_{t_0}^{t_f} 2\Gamma(t) dt \right] \equiv M_{\text{v}}^0 \exp \left[2\overline{\Gamma(t)} \cdot t_{\text{grow}} \right], \quad (75)$$

with M_{v}^0 the initial condensate mass as a seed for the growing, $t_{0,f}$ corresponding to $M_{0,f}$, $t_{\text{grow}} \equiv t_f - t_0$ the total growth time, and $\overline{\Gamma(t)}$ an effective averaged superradiance rate over the integrated time interval. Since $\Gamma(t)$ evolves with time following Equation (5) and Figure II, generally t_{grow} is hard to obtain analytically, while a commonly used approximation is done by replacing $2\overline{\Gamma(t)}$ by the fastest energy density growth rate as a constant, e.g., $\Gamma_{\text{sr}} \sim 4\chi\alpha^6\mu$ for vector clouds [54] leading to the typical superradiance time as $\tau_{\text{sr}} \equiv 1/\Gamma_{\text{sr}} = M/(4\chi\alpha^7)$, thus a simplified analytical superradiance time is shown as

$$t_{\text{sr}} \simeq \tau_{\text{sr}} \log \left(\frac{M_{\text{v}}^{\text{max}}}{M_{\text{v}}^0} \right), \quad (76)$$

with the typical time τ_{sr} about seconds to minutes for vector clouds around a stellar mass BH, and the exponential growth time t_{sr} approximately 2 orders of magnitude larger due to the logarithm amplification and can last for hours. Straightforward as we just stated, an increase of $2\overline{\Gamma(t)}$ by substitution would certainly underestimate the value of t_{grow} , so

$$\tau_{\text{sr}} < t_{\text{sr}} < t_{\text{grow}}, \quad (77)$$

we will directly read t_{grow} from numerics afterwards in the next subsection.

During the process throughout, GW emission via annihilations occurs, $\dot{E}_{\text{GW}} = \Gamma_{\text{ann}} M_{\text{v}}^2$, which is however subdominant in the previous superradiant stage; after the condensate reaches its maximum $\Gamma \rightarrow 0$, it becomes dominant in the evolution Eq (74), then the system gradually depletes its energy and undergoes the decay stage. The leading term of the GW flux in this stage is obtained by fitting numerics to the condensate mass squared proportionality, which in the small coupling limit reads

$$\lim_{\alpha \ll 1} \dot{E}_{\text{GW}} \approx C_{\text{GW}} \left(\frac{M_{\text{v}}}{M_f} \right)^2 \alpha_f^{10}. \quad (78)$$

where $\alpha_f \equiv \mu M_f$ with M_f the final BH mass at the saturation. The coefficient C_{GW} is estimated to be 6.4 and 60 in flat and Schwartzchild geometry respectively, we adopt the value of 16.66 [107] in this study, while the latest simulation gives 27.16 in a recent work [73]. The evolution in this stage is solved by

$$M_v = \frac{M_v^{\max}}{1 + \Gamma_{\text{ann}} M_v^{\max} t}, \quad (79)$$

with the typical timescale defined to be the “half-time” of the condensate,

$$\tau_{\text{GW}} \equiv \frac{1}{\Gamma_{\text{ann}} M_v^{\max}} = \frac{M_v}{\dot{E}_{\text{GW}}^0} \approx \frac{1}{C_{\text{GW}}} \frac{M_f^2}{M_v^{\max}} \alpha_f^{-10}, \quad (80)$$

where \dot{E}_{GW}^0 is evaluated at $M_v = M_v^{\max}$ in Eq (78). A direct numerical evaluation shows that τ_{GW} significantly exceeds t_{grow} , as will be shown in Table III. Consequently, the depletion of the condensate mass due to GW emission becomes dominant for a much longer timescale than the superradiance stage, consistent with timescales that would be shown in Fig. V.

Back to the superradiant stage, with the suppression of GW emissions, analytical approximations can be done at the saturation time, when the BH mass and spin of decrease from their initial values M_0 and χ_0 to their final values M_f and χ_f . The relations $\Delta M = \omega \Delta J$ and $\omega = \Omega_{\text{H}}$ directly yields

$$\begin{cases} M_v^{\max} = M_0 - M_f = \mu (\chi_0 M_0^2 - \chi_f M_f^2) \\ \chi_f = \frac{4\mu M_f}{1 + 4(\mu M_f)^2}, \end{cases} \quad (81)$$

with $\omega \approx \mu$ used. When initial states (M_0, χ_0) are given, the two unknowns (M_f, χ_f) are solved with the above two equations. In the small coupling $\alpha \equiv M\mu < 0.5$ and small energy extraction efficiency $\beta \equiv M_v^{\max}/M_0 < 0.3$ limits, the joining equation of the above two,

$$\beta = \alpha_0(\chi_0 - \chi_f) + 2\alpha_0\chi_f\beta - \alpha_0\chi_f\beta^2 \quad (82)$$

is simplified by dropping higher order terms to reach

$$\beta = \alpha_0(\chi_0 - 4\alpha_0), \quad (83)$$

which solely determines the final state, in a modest accuracy [67]. This quantitative approximation holds true for cases with or without reflection, while the effect of reflection manifests itself by accelerating or decelerating the superradiant growth. If the initial state of the bounded system satisfy the anomaly criteria (65), the reflection parameter enhances the superradiance for a period of time, otherwise the

superradiance will be attenuated. The system evolutions are illustrated by solving Eqs. (72) numerically and results are shown in Fig. V, and the growth rates of the condensates over time for different BH spins and reflections are shown in Fig. VI.

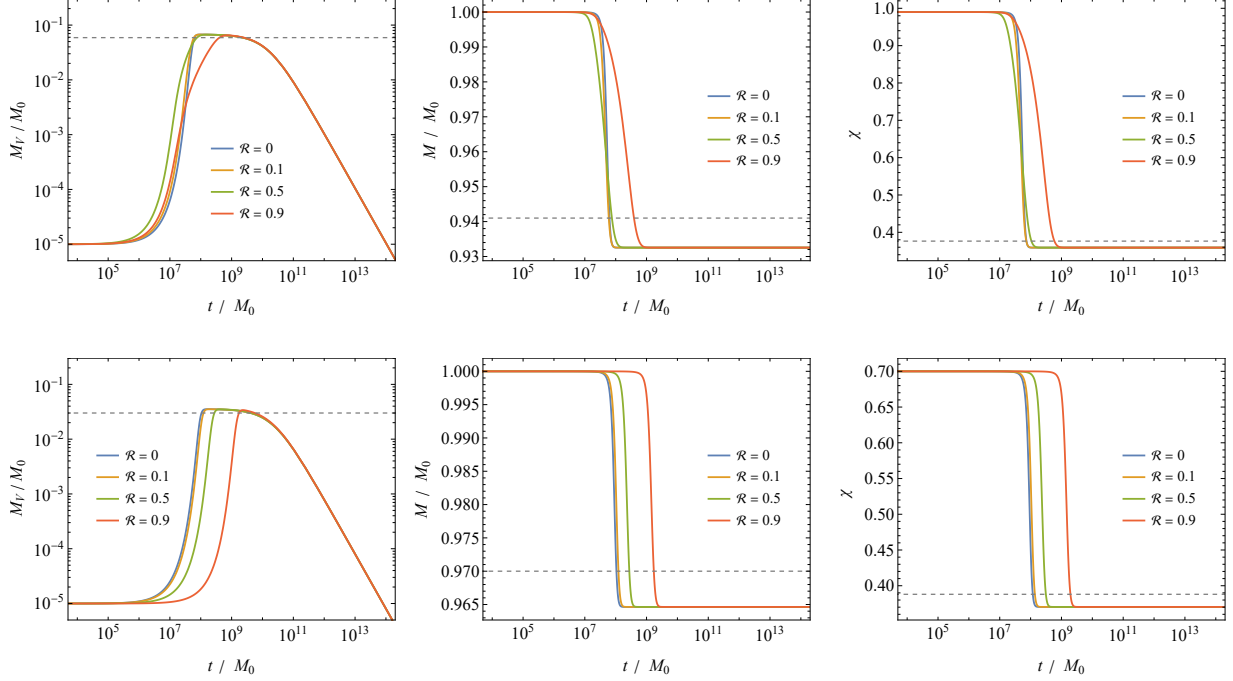


FIG. V. The evolution of the BH-condensate system with different reflection parameters \mathcal{R} . Only the mode $\{1, 0, 1, 1\}$ is considered in the condensate. The initial BH spins are $\chi_0 = 0.99$ for the top figure and 0.7 for the bottom figure. The panels from left to right illustrate the condensate mass, BH mass, and BH spin, respectively. The dashed lines in the panels label the estimations of the maximum condensate masses, the final BH masses, and the final BH spins, i.e. Eqs. (81-83). The initial mass coupling is $\alpha_0 = 0.1$ and the initial mass of the condensate M_V^0 is set to be $10^{-5}M_0$.

As we can see from Fig V, for the case in which the BH spin is smaller than the critical spin, e.g., $\chi_0 = 0.7 < 1/\sqrt{2}$ (bottom figure), the superradiant stage is delayed monotonically as the reflection parameter becomes larger; for the extreme case of $\chi_0 = 0.99$ (top figure), the cases with reflection exhibit accelerated growth rates of the condensate mass at the beginning of the superradiance, and a deceleration in growth rates afterwards. The comparison of these growth rates is demonstrated more clearly in Fig. VI, where we denote anomalous enhancement in the purple dashed box.

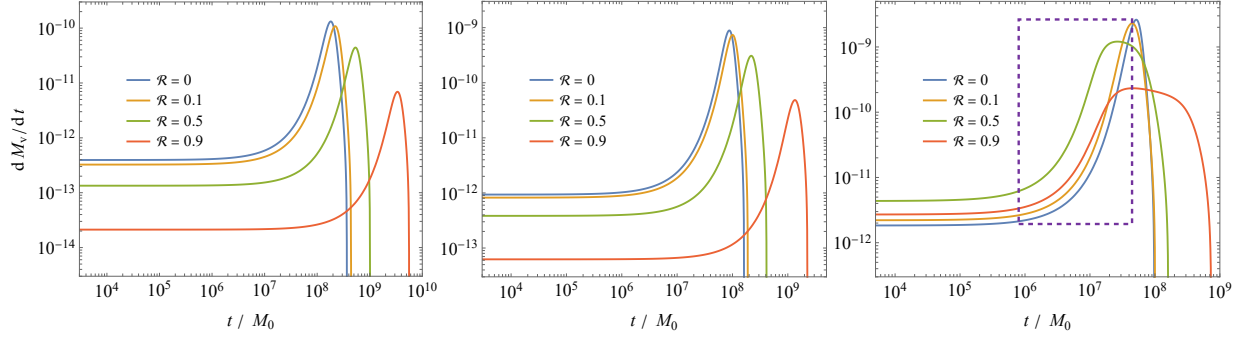


FIG. VI. The growth rates of the condensate mass over time for the $\{1, 0, 1, 1\}$ mode. Initial BH spins are $\chi = 0.5$ (left panel), $\chi = 1/\sqrt{2}$ (middle panel) and $\chi = 0.99$ (right panel). The initial mass coupling is $\alpha_0 = 0.1$, and the initial condensate mass is $10^{-5}M_0$. The dashed box marks part of the region where growth is faster for all the values chosen of \mathcal{R} when $\chi_0 = 0.99$.

However, even if the reflection parameter may enhance the superradiance over some time, the time to reach the final state is always delayed, as can be seen in Fig. V the time when M_v reaches its max, and in Fig. VI the time when $dM_v/dt = 0$. So here we make an interesting metaphor for the anomalous phenomenon we’ve found, which is described as a race between “The Tortoise and the Hare”: generally as the reflection parameter \mathcal{R} becomes larger, the instability rate Γ gradually decays to 0, which intuitively recovers stability as boundary condition tends to be regular, this is the “tortoise” we originally have; but what we’ve found in high spin BH case is a temporally running faster “hare”, which brings a larger instability rate as \mathcal{R} increases due to Eq. (65), but takes a slack afterwards and finally reaches the almost same final state with a time delay (see Fig VII for a carton animation generated by DALL-E, OpenAI). In the superradiant stage, this would have impacts on the GW emission power and the GW strain, but with only the later an observable, which is quantified in the next subsection. We will also postulate a physical interpretation for this anomaly in the discussion, which is to be verified/falsified and formulated in the future study.



FIG. VII. A carton animation of the superradiant anomalous growth—“The Tortoise and the Hare”, generated by DALL-E, OpenAI.

B. Anomaly features and GW strain magnification

In order to gain a more quantitatively description of the reflection-induced growth anomaly, in addition to the above quantities that generally describe the evolution, we introduce three additional characteristic quantities. These quantities specifically focus on the system with reflection in the anomalous scenario, where reflection amplifies superradiant growth. The first quantity is $(\Delta\dot{M}_v)_{\max}$, which corresponds to the maximum growth rate difference at a same instant between the reflective and non-reflective system. It demonstrates the utmost extent of reflection to enhance the growth rate throughout the evolution. The second quantity is denoted as $(\Delta M_v)_{\max}$, the maximum condensate mass difference between systems with and without reflection. It quantifies the peak advantage in the condensate mass of the reflective system compared to its non-reflective counterpart. The third quantity t_{adv} gives the period of time during which the reflective system retains its condensate mass advantage, before being overtaken by the non-reflective system.³ In Tab. III, we present these quantities for the case $\chi_0 = 0.99$ where the anomaly is most obvious. The numerical value of t_{grow} indicates that the typical timescales extend with increasing reflection, suggesting that reflection ultimately slows down superradiant growth. On the other hand, both $(\Delta\dot{M}_v)_{\max}$ and $(\Delta M_v)_{\max}$ reveal that every reflective system experiences a phase where its growth is enhanced by reflection. These systems maintain a condensate mass advantage for a duration t_{adv} , which decreases as the reflection intensifies.

We can also compute the characteristic quantities in SI units, taking a stellar BH with its mass $M_0 = 100M_\odot$ and the reflection parameter $\mathcal{R} = 0.5$ as an example. In this case, the maximum growth rate difference is given by $(\Delta\dot{M}_v)_{\max} = 2.49 \times 10^{26} \text{ kg} \cdot \text{s}^{-1}$, which is approximately $10^{-4}M_\odot$ (about 100 times the mass of the Earth) per second. The maximum difference in condensate mass is $(\Delta M_v)_{\max} = 4.30 \times 10^{30} \text{ kg}$ or $2.16M_\odot$, and the advantage time is $t_{\text{adv}} = 2.79 \times 10^4 \text{ s}$, or 7.75 hours (anomaly signal duration). For more massive BHs, the maximum growth rate difference $(\Delta\dot{M}_v)_{\max}$ remains unchanged because the superradiant instability is not solely dependent on M . However, both the maximum condensate mass difference $(\Delta M_v)_{\max}$ and the advantage time increase t_{adv} as the BH mass becomes greater.

As we've mentioned, the reflection-induced superradiant anomalous growth should have impacts on both GW power and strain, while in a previous numerical work for the scalar case [97], the authors pointed out the change in the GW emission rate due to reflection is only obvious for high mass couplings

³ Note that by definition, $t_{\text{adv}} < t_{\text{grow}}$ is consistent with numerics in Tab. III, but there is possibility for t_{adv} greater than t_{sr} defined in Eq. (76), which is an analytical approximation.

χ_0	\mathcal{R}	General evolution quantities				Anomaly features		
		$M_f(M_v^{\max})/M_0$	χ_f	t_{GW}/M_0	t_{grow}/M_0	$(\Delta\dot{M}_v)_{\max}$	$(\Delta M_v)_{\max}/M_0$	t_{adv}/M_0
0.99	0				9.79×10^7	-	-	-
	0.1	0.941(0.059)	0.376	1.66×10^{10}	1.01×10^8	3.23×10^{-10}	1.36×10^{-2}	7.70×10^7
	0.5				1.61×10^8	6.16×10^{-10}	2.16×10^{-2}	5.66×10^7
	0.9				7.36×10^8	4.06×10^{-11}	9.36×10^{-4}	3.27×10^7

TABLE III. The general quantities, as well as the characteristic quantities showing the anomaly features for different reflection parameters, with initial mass coupling $\alpha_0 = 0.1$, initial condensate mass $M_{v,0} = 10^{-5}M_0$, and initial BH spin $\chi_0 = 0.99$. M_v^{\max} is the maximum mass of the vector condensate. M_f and χ_f are the final BH mass and spin. t_{GW} is the characteristic timescale for the GW emission of the condensate, i.e., the time when the condensate decays to half of M_v^{\max} . t_{grow} is the duration of superradiant growth of the condensate. $(\Delta\dot{M}_v)_{\max}$ is the maximum difference in growth rate between the systems with and without reflection. $(\Delta M_v)_{\max}$ is the maximum difference in the condensate mass between the systems with and without reflection. t_{adv} is the time span during which the system with reflection maintains its condensate mass advantage before being overtaken by the system without reflection.

($\alpha \gtrsim 0.5$), which is beyond the superradiant domain ($\alpha \lesssim 0.5$); however, they only considered cases as the reflection parameter \mathcal{R} close to 0 or 1, for intermediate values in $(0, 1)$, where our anomalous growth sets in, the reflection does have a theoretical possibility to influence the GW power and the GW strain, with the later an observable, thus it's worth formulating and featuring this anomaly. The GW strain amplitude is expressed in terms of the energy flux as [64]

$$h = \sqrt{\frac{4}{\omega_{\text{ann}}^2 r^2} \dot{E}_{\text{GW}}} \quad (84)$$

for a source made up of bosonic condensate annihilating in the corresponding mode, $\omega_{\text{ann}} \simeq 2\mu$, emitting power \dot{E}_{GW} at a distance r away from the Earth. In joint with the vector annihilation term, we have

$$h_v(t) = M_v(t) \sqrt{\frac{4}{\omega_{\text{ann}}^2 r^2} \Gamma_{\text{ann}}}, \quad (85)$$

the direct proportionality $h_v \propto M_v$ allows us to characterize the anomalous growth of the condensate into the GW strain. Invoking the exponential growth of the condensate, see Eq. (75), we propose the signal ratio $r_h(\mathcal{R}, t)$ of the reflection-induced GW strain with that of the case with no reflection,

$$r_h(\mathcal{R}, t) = \frac{h_v(\mathcal{R}, t)}{h_v(\mathcal{R} = 0, t)} = \frac{M_v(\mathcal{R}, t)}{M_v(\mathcal{R} = 0, t)} = \exp \left\{ \int_{t_0}^t 2\bar{\Gamma}(\mathcal{R}, u) [f(\mathcal{R}, u) - 1] du \right\}, \quad (86)$$

with t the measured time instant to see the signal ratio. As such, the featured quantities we proposed can be expressed as

$$\begin{cases} \frac{\Delta \dot{M}_v(\mathcal{R}, t)}{\dot{M}_v(\mathcal{R} = 0, t)} = f(\mathcal{R}, t)r_h(\mathcal{R}, t) - 1 \\ \frac{\Delta M_v(\mathcal{R}, t)}{M_v(\mathcal{R} = 0, t)} = r_h(\mathcal{R}, t) - 1, \end{cases} \quad (87)$$

so we could identify that the time instant for $(\Delta \dot{M}_v)_{\max}$ to take place corresponds to the maximum anomalous growth rate $[f(\mathcal{R}, t)]_{\max}$ and a still enhancing signal ratio $\dot{r}_h(\mathcal{R}, t) > 0$; the time instant for $(\Delta M_v)_{\max}$ to take place corresponds to $f(\mathcal{R}, t) = 1$ and $[r_h(\mathcal{R}, t)]_{\max}$, when the GW strain with reflection is most distinguishable; t_{adv} is time when $f(\mathcal{R}, t) < 1$ and $r_h(\mathcal{R}, t) = 1$, the GW strains return the same, and anomalous signal ends. So in a time-sequent order, we have $t_{(\Delta \dot{M}_v)_{\max}} < t_{(\Delta M_v)_{\max}} < t_{\text{adv}}$.

To find the most significant signal ratio with respect to reflection, we assume the measured time is short during the evolution, which is consistent with the high BH spin and low saturation conditions to allow anomaly, such that

$$r_h(\mathcal{R}, t) \approx 1 + \int_{t_0}^t 2\bar{\Gamma}(u) [f(\mathcal{R}, u) - 1] du, \quad (88)$$

further, as we see in Fig V, the anomaly is mostly obvious in the fastest growing superradiant stage, thus the superradiance rate is set to be the fastest rate $2\bar{\Gamma}(t) \rightarrow \Gamma_{\text{sr}}$, and time interval is meanwhile selected as $t_H - t_0 \rightarrow \tau_{\text{sr}}$, so

$$r_h(\mathcal{R}, t) \approx 1 + \Gamma_{\text{sr}}\tau_{\text{sr}} [f(\mathcal{R}, t) - 1] = f(\mathcal{R}, t), \quad (89)$$

where $\Gamma_{\text{sr}}\tau_{\text{sr}} = 1$ is by definition. We see that the modifier $f(\mathcal{R}, t)$ itself is the magnification of the GW strain, in the earliest stage of the evolution. Meanwhile the GW power \dot{E}_{GW} naturally scales as $f^2(\mathcal{R}, t)$, which is however not an observable. The maximum value of the modifier $f(\mathcal{R}, t)$ with respect to the reflection takes place at \mathcal{R}_c , expressed in Equation (66); and we read numerically from Figure III, when $\chi = 0.99$ and $\omega/\Omega_H = 0.01$, the reflection-induced GW strain magnification is about $r_h(\mathcal{R}, t) \approx f(\mathcal{R} \simeq 0.75) \simeq 3.5$ times.

Further, by an analogous analysis, joining with Eqs. (4) and (5), the ratio between the strains of vector and scalar/tensor dominant modes with the same reflection reads

$$\frac{h_v(\mathcal{R})}{h_{s/t}(\mathcal{R})} \approx \frac{\Gamma_v}{\Gamma_{s/t}} \approx \alpha^{-2} \simeq 2500 \left(\frac{3M_{\odot}}{M} \right)^2 \left(\frac{10^{-12}\text{eV}}{\mu} \right)^2 \quad (90)$$

Just as we stated in the introduction, vector dominant mode serves as the best candidate to characterize effects by reflection, which is mostly obvious in Tab. I, and Fig. I. The reflection-induced anomalous

enhancement r_h of the signal strain, together with the α^{-2} coupling power magnification for vector case, is distinguishable if we are lucky enough to catch the moment when a highly spinning Kerr BH captures a small amount of ultralight bosons to begin superradiance, providing an opportunity to shed lights on the micro-structure of the BH horizon.

V. CONCLUSION AND DISCUSSION

In this study, we investigate the effects of near-horizon reflection of a Kerr BH on the superradiance process and evolution of spin-1 vector bosonic condensate, with the dominant $|1011\rangle$ mode the most sensitive to horizon geometry and fastest growing mode among the scalar, vector and tensor states, it transfers the BH spin into the intrinsic spin of field rather than the orbital angular momentum, which is a distinguishable feature from the vastly studied scalar case. Hydrogenic structures exhibit in the near-flat spacetime and in the far zone, providing the source for monochromatic GW emissions via energy level transitions and annihilations. In the full analytical treatment, due to the existence of additional poles, three pieces of radial asymptotic solutions should be matched, which is done in the leading order of the angular part; in the solution, we optimize the matching procedure by using a different basis which naturally corresponds to the ingoing and outgoing flux and saves from the switching between different basis as that in many of the previous studies. The near-horizon reflection is denoted by a parameter \mathcal{R} , which we restrict to be a real value; we studied the modifications due to the reflection parameter on the complex energy level and hence on the superradiance rate, which was plotted in terms of the mass coupling using analytical and numerical results, which have consistent behaviors in the $\alpha \ll 1$ limit. By careful observations, we find that generally as the reflection parameter goes up from 0 to 1, the superradiance rate monotonically decreases, while in the early stage of high-spin BH case, the superradiance rate could temporarily increase with \mathcal{R} , and then decays to vanish as usual. This peculiar situation also occurs in the scalar cases studied earlier, but lacks a substantial treatment, and it's moreover magnified in the dominant vector case hence deserves a formal analysis; we identified this phenomenon as the “anomalous growth” of the superradiant condensate, and by singling out the modifier, we figured out the anomaly conditions in three forms: (1) the mathematical form describes well with the figures where we found the situation, which meanwhile gives the critical reflection for the best optimization; (2) the geometrical form goes with two induced angles, which elegantly shows the anomaly in a clock-like diagram with two pointers denoting the superradiance state and the reflection state; (3) the physical form relates the anomaly with the entropy and information carried

away by unit superradiant particle, which is a manifestation of rotation-relativistic of fast-spinning BH and deserves deeper investigations in the future once we complement physics of the reflection side. Then, we proceeded with the study of the whole system's evolution, by considering energy and angular momentum exchange among the BH, the condensate and the GWs. We found that although the anomalous growth could temporarily increase the superradiance with reflection, the time for the condensate to reach the maximum is always delayed for a larger reflection parameter. So we make a metaphor for the phenomenon as a race between “the Tortoise and the Hare”, with the former the attenuation of superradiant growth by a higher reflection in a low-spin BH case, and the later the temporarily elevated and then descended growth rate by a higher reflection in a fast-spin BH case. Further, we proposed three featured quantities to characterize the anomaly: the maximum growth difference, the maximum condensate mass difference, and the advantage time for the anomaly, and we showed the numerics for the case $\chi_0 = 0.99$ when the anomaly is very obvious; in a reasonable numerical estimate, these quantities are considerable in SI units. We further related the three quantities to the signal ratio of the GW strain, identified the time-sequent order of the corresponding instants; also we checked the effect of reflection on the GW strain, finding that the modifier is itself the magnification factor in the early stage of the evolution, with the best scenario 3.5 times as the strain without reflection. Although the GW in the earliest superradiance stage is relatively weak, if we were lucky enough to catch a highly-spinning BH capturing a seed of the condensate, it will shed light on the microstructure and quantum nature of the BH horizon.

However, along with the potential implications of the three forms of anomaly condition we proposed, a possible physical explanation is yet to be explored. We preliminarily postulate a possibility: the existence of reflection term plays two roles, one of which is to occupy the negative energy orbits which leads to attenuating the instability rate, the other is to release negative energy states by modify the BH area thus enlarging the ergosphere volume; the two effects complete with each other, with the former magnificent in relatively slowly rotating BH case, while the later only manifestly shows in the relativistic fast-spinning BH case. Yet, this explanation deserves a further verification/falsification and formulating, which we leave in the future study.

On the other hand, we restricted the reflection parameters to real-valued constants, while introducing detailed quantum-corrected models could yield more complex effects on superradiant rates and evolution. In particular, since superradiant anomaly we've found gives the non-monotonicity dependence on reflection, a specific reflection spectrum would support a certain intermediate value of boson mass,

rather than the lightest or heaviest, to produce the most significant GW signal from condensates around high spin BHs. We will report this mass selection procedure along our research line in the future.

The superradiant growth anomaly, is expected to be more magnificent in the tensor polar dipole mode, due to the alleviation of the α -suppression, which is however non-hydrogenic type; and the generalization in the charged case deserves an attentive treatment, which is although less astronomically relevant. The electromagnetic signal features of the growth anomaly is also of potential interest, as it provides wider observational possibilities other than GWs. Our conclusions may also be extended to more complicated astrophysical environments, such as in cases of accretion, self-interaction, and bosonovas etc. Additional investigations into cases including the presence of a companion star, or considering more types of exotic compact objects (ECOs) as the central body of the system, may also provide comprehensive insights.

ACKNOWLEDGEMENTS

We give special thanks to Prof. Hong Zhang and Prof. Shou-Shan Bao for their warm hospitality in Shandong University where part of N. Jia's work has been done, and give thanks to Mr. Jiangyuan Qian and Dr. Bing Sun for their valuable suggestions and assistance in the early stage of this study. We give additional thanks to Dr. Rong-Zhen Guo and Prof. Qing-Guo Huang for their help in our understanding the asymptotic expansions of some special functions, and give thanks to Prof. Lijing Shao for his expertise in support for our research. The starting work of N. Jia and G-R. Liang is supported by the National Natural Science Foundation of China (Grants Nos. 12147163 and 12175099), the remaining work of G-R. Liang is supported by Jiangsu Funding Program for Excellent Postdoctoral Talent; the work of Y-D. Guo is supported by the National Natural Science Foundation of China (Grant No. 12075136) and the Natural Science Foundation of Shandong Province (Grant No. ZR2020MA094); the work of Z-F. Mai is supported by the National Natural Science Foundation of China (Grants No. 12247128); the work of X. Zhang is supported by the National Natural Science Foundation of China (Grants Nos. 11975072, 11835009, and 12473001), the National SKA Program of China (Grants Nos. 2022SKA0110200 and 2022SKA0110203), and the 111 Project (Grant No. B16009).

-
- [1] Asimina Arvanitaki, Savas Dimopoulos, Sergei Dubovsky, Nemanja Kaloper, and John March-Russell, “String Axiverse,” *Phys. Rev. D* **81**, 123530 (2010), [arXiv:0905.4720 \[hep-th\]](#).
 - [2] Rouven Essig et al., “Working Group Report: New Light Weakly Coupled Particles,” in *Snowmass 2013: Snowmass on the Mississippi* (2013) [arXiv:1311.0029 \[hep-ph\]](#).

- [3] Igor G. Irastorza and Javier Redondo, “New experimental approaches in the search for axion-like particles,” *Prog. Part. Nucl. Phys.* **102**, 89–159 (2018), [arXiv:1801.08127 \[hep-ph\]](#).
- [4] Peter W. Graham, Jeremy Mardon, and Surjeet Rajendran, “Vector Dark Matter from Inflationary Fluctuations,” *Phys. Rev. D* **93**, 103520 (2016), [arXiv:1504.02102 \[hep-ph\]](#).
- [5] Prateek Agrawal, Naoya Kitajima, Matthew Reece, Toyokazu Sekiguchi, and Fuminobu Takahashi, “Relic Abundance of Dark Photon Dark Matter,” *Phys. Lett. B* **801**, 135136 (2020), [arXiv:1810.07188 \[hep-ph\]](#).
- [6] D. Antypas *et al.*, “New Horizons: Scalar and Vector Ultralight Dark Matter,” (2022), [arXiv:2203.14915 \[hep-ex\]](#).
- [7] John Preskill, Mark B. Wise, and Frank Wilczek, “Cosmology of the Invisible Axion,” *Phys. Lett. B* **120**, 127–132 (1983).
- [8] L. F. Abbott and P. Sikivie, “A Cosmological Bound on the Invisible Axion,” *Phys. Lett. B* **120**, 133–136 (1983).
- [9] Michael Dine and Willy Fischler, “The Not So Harmless Axion,” *Phys. Lett. B* **120**, 137–141 (1983).
- [10] Peter Svrcek and Edward Witten, “Axions In String Theory,” *JHEP* **06**, 051 (2006), [arXiv:hep-th/0605206](#).
- [11] Asimina Arvanitaki and Sergei Dubovsky, “Exploring the String Axiverse with Precision Black Hole Physics,” *Phys. Rev. D* **83**, 044026 (2011), [arXiv:1004.3558 \[hep-th\]](#).
- [12] Richard Brito, Vitor Cardoso, and Paolo Pani, “Superradiance: New Frontiers in Black Hole Physics,” *Lect. Notes Phys.* **906**, pp.1–237 (2015), [arXiv:1501.06570 \[gr-qc\]](#).
- [13] David J. E. Marsh, “Axion Cosmology,” *Phys. Rept.* **643**, 1–79 (2016), [arXiv:1510.07633 \[astro-ph.CO\]](#).
- [14] Lam Hui, Jeremiah P. Ostriker, Scott Tremaine, and Edward Witten, “Ultralight scalars as cosmological dark matter,” *Phys. Rev. D* **95**, 043541 (2017), [arXiv:1610.08297 \[astro-ph.CO\]](#).
- [15] Lorenzo Annulli, Vitor Cardoso, and Rodrigo Vicente, “Response of ultralight dark matter to supermassive black holes and binaries,” *Phys. Rev. D* **102**, 063022 (2020), [arXiv:2009.00012 \[gr-qc\]](#).
- [16] Francesca Chadha-Day, John Ellis, and David J. E. Marsh, “Axion dark matter: What is it and why now?” *Sci. Adv.* **8**, abj3618 (2022), [arXiv:2105.01406 \[hep-ph\]](#).
- [17] Hooman Davoudiasl, Peter B. Denton, and David A. McGady, “Ultralight fermionic dark matter,” *Phys. Rev. D* **103**, 055014 (2021), [arXiv:2008.06505 \[hep-ph\]](#).
- [18] C. B. Adams *et al.*, “Axion Dark Matter,” in *Snowmass 2021* (2022) [arXiv:2203.14923 \[hep-ex\]](#).
- [19] Bohua Li, Tanja Rindler-Daller, and Paul R. Shapiro, “Cosmological Constraints on Bose-Einstein-Condensed Scalar Field Dark Matter,” *Phys. Rev. D* **89**, 083536 (2014), [arXiv:1310.6061 \[astro-ph.CO\]](#).
- [20] R. D. Peccei and Helen R. Quinn, “CP Conservation in the Presence of Instantons,” *Phys. Rev. Lett.* **38**, 1440–1443 (1977).
- [21] Frank Wilczek, “Axions and Family Symmetry Breaking,” *Phys. Rev. Lett.* **49**, 1549–1552 (1982).
- [22] Y. Chikashige, Rabindra N. Mohapatra, and R. D. Peccei, “Are There Real Goldstone Bosons Associated with Broken Lepton Number?” *Phys. Lett. B* **98**, 265–268 (1981).

- [23] Viraf M. Mehta, Mehmet Demirtas, Cody Long, David J. E. Marsh, Liam Mcallister, and Matthew J. Stott, “Superradiance Exclusions in the Landscape of Type IIB String Theory,” (2020), [arXiv:2011.08693 \[hep-th\]](#).
- [24] Emanuele Berti *et al.*, “Testing General Relativity with Present and Future Astrophysical Observations,” *Class. Quant. Grav.* **32**, 243001 (2015), [arXiv:1501.07274 \[gr-qc\]](#).
- [25] Thomas P. Sotiriou and Valerio Faraoni, “Black holes in scalar-tensor gravity,” *Phys. Rev. Lett.* **108**, 081103 (2012), [arXiv:1109.6324 \[gr-qc\]](#).
- [26] Lotty Ackerman, Matthew R. Buckley, Sean M. Carroll, and Marc Kamionkowski, “Dark Matter and Dark Radiation,” *Phys. Rev. D* **79**, 023519 (2009), [arXiv:0810.5126 \[hep-ph\]](#).
- [27] Kazunori Nakayama, “Vector Coherent Oscillation Dark Matter,” *JCAP* **10**, 019 (2019), [arXiv:1907.06243 \[hep-ph\]](#).
- [28] Mark Goodsell, Joerg Jaeckel, Javier Redondo, and Andreas Ringwald, “Naturally Light Hidden Photons in LARGE Volume String Compactifications,” *JHEP* **11**, 027 (2009), [arXiv:0909.0515 \[hep-ph\]](#).
- [29] Joerg Jaeckel and Andreas Ringwald, “The Low-Energy Frontier of Particle Physics,” *Ann. Rev. Nucl. Part. Sci.* **60**, 405–437 (2010), [arXiv:1002.0329 \[hep-ph\]](#).
- [30] Pablo G. Camara, Luis E. Ibanez, and Fernando Marchesano, “RR photons,” *JHEP* **09**, 110 (2011), [arXiv:1106.0060 \[hep-th\]](#).
- [31] Alfred Scharff Goldhaber and Michael Martin Nieto, “Photon and Graviton Mass Limits,” *Rev. Mod. Phys.* **82**, 939–979 (2010), [arXiv:0809.1003 \[hep-ph\]](#).
- [32] [Fundamental Physics at the Intensity Frontier](#) (2012) [arXiv:1205.2671 \[hep-ex\]](#).
- [33] Kurt Hinterbichler, “Theoretical Aspects of Massive Gravity,” *Rev. Mod. Phys.* **84**, 671–710 (2012), [arXiv:1105.3735 \[hep-th\]](#).
- [34] Claudia de Rham, “Massive Gravity,” *Living Rev. Rel.* **17**, 7 (2014), [arXiv:1401.4173 \[hep-th\]](#).
- [35] Renée Hlozek, Daniel Grin, David J. E. Marsh, and Pedro G. Ferreira, “A search for ultralight axions using precision cosmological data,” *Phys. Rev. D* **91**, 103512 (2015), [arXiv:1410.2896 \[astro-ph.CO\]](#).
- [36] Olaf Baake and Oliver Rinne, “Superradiance of a charged scalar field coupled to the Einstein-Maxwell equations,” *Phys. Rev. D* **94**, 124016 (2016), [arXiv:1610.08352 \[gr-qc\]](#).
- [37] William H. Press and Saul A. Teukolsky, “Floating Orbits, Superradiant Scattering and the Black-hole Bomb,” *Nature* **238**, 211–212 (1972).
- [38] Vitor Cardoso, Oscar J. C. Dias, Jose P. S. Lemos, and Shijun Yoshida, “The Black hole bomb and superradiant instabilities,” *Phys. Rev. D* **70**, 044039 (2004), [Erratum: *Phys.Rev.D* 70, 049903 (2004)], [arXiv:hep-th/0404096](#).
- [39] S. W. Hawking and H. S. Reall, “Charged and rotating AdS black holes and their CFT duals,” *Phys. Rev. D* **61**, 024014 (2000), [arXiv:hep-th/9908109](#).

- [40] Vitor Cardoso, Oscar J. C. Dias, and Shijun Yoshida, “Classical instability of Kerr-AdS black holes and the issue of final state,” *Phys. Rev. D* **74**, 044008 (2006), [arXiv:hep-th/0607162](#).
- [41] Nami Uchikata, Shijun Yoshida, and Toshifumi Futamase, “Scalar perturbations of Kerr-AdS black holes,” *Phys. Rev. D* **80**, 084020 (2009).
- [42] Daniel Baumann, Horng Sheng Chia, John Stout, and Lotte ter Haar, “The Spectra of Gravitational Atoms,” *JCAP* **12**, 006 (2019), [arXiv:1908.10370 \[gr-qc\]](#).
- [43] T. Damour, N. Deruelle, and R. Ruffini, “On Quantum Resonances in Stationary Geometries,” *Lett. Nuovo Cim.* **15**, 257–262 (1976).
- [44] T. J. M. Zouros and D. M. Eardley, “INSTABILITIES OF MASSIVE SCALAR PERTURBATIONS OF A ROTATING BLACK HOLE,” *Annals Phys.* **118**, 139–155 (1979).
- [45] Steven L. Detweiler, “KLEIN-GORDON EQUATION AND ROTATING BLACK HOLES,” *Phys. Rev. D* **22**, 2323–2326 (1980).
- [46] Sam R. Dolan, “Instability of the massive Klein-Gordon field on the Kerr spacetime,” *Phys. Rev. D* **76**, 084001 (2007), [arXiv:0705.2880 \[gr-qc\]](#).
- [47] Yakov Shlapentokh-Rothman, “Exponentially growing finite energy solutions for the Klein-Gordon equation on sub-extremal Kerr spacetimes,” *Commun. Math. Phys.* **329**, 859–891 (2014), [arXiv:1302.3448 \[gr-qc\]](#).
- [48] Paolo Pani, Vitor Cardoso, Leonardo Gualtieri, Emanuele Berti, and Akihiro Ishibashi, “Black hole bombs and photon mass bounds,” *Phys. Rev. Lett.* **109**, 131102 (2012), [arXiv:1209.0465 \[gr-qc\]](#).
- [49] Paolo Pani, Vitor Cardoso, Leonardo Gualtieri, Emanuele Berti, and Akihiro Ishibashi, “Perturbations of slowly rotating black holes: massive vector fields in the Kerr metric,” *Phys. Rev. D* **86**, 104017 (2012), [arXiv:1209.0773 \[gr-qc\]](#).
- [50] Helvi Wittek, Vitor Cardoso, Akihiro Ishibashi, and Ulrich Sperhake, “Superradiant instabilities in astrophysical systems,” *Phys. Rev. D* **87**, 043513 (2013), [arXiv:1212.0551 \[gr-qc\]](#).
- [51] Richard Brito, Vitor Cardoso, and Paolo Pani, “Massive spin-2 fields on black hole spacetimes: Instability of the Schwarzschild and Kerr solutions and bounds on the graviton mass,” *Phys. Rev. D* **88**, 023514 (2013), [arXiv:1304.6725 \[gr-qc\]](#).
- [52] William E. East, “Superradiant instability of massive vector fields around spinning black holes in the relativistic regime,” *Phys. Rev. D* **96**, 024004 (2017), [arXiv:1705.01544 \[gr-qc\]](#).
- [53] William E. East and Frans Pretorius, “Superradiant Instability and Backreaction of Massive Vector Fields around Kerr Black Holes,” *Phys. Rev. Lett.* **119**, 041101 (2017), [arXiv:1704.04791 \[gr-qc\]](#).
- [54] Masha Baryakhtar, Robert Lasenby, and Mae Teo, “Black Hole Superradiance Signatures of Ultralight Vectors,” *Phys. Rev. D* **96**, 035019 (2017), [arXiv:1704.05081 \[hep-ph\]](#).
- [55] Vitor Cardoso, Óscar J. C. Dias, Gavin S. Hartnett, Matthew Middleton, Paolo Pani, and Jorge E. Santos, “Constraining the mass of dark photons and axion-like particles through black-hole superradiance,” *JCAP* **03**, 043 (2018), [arXiv:1801.01420 \[gr-qc\]](#).

- [56] William E. East, “Massive Boson Superradiant Instability of Black Holes: Nonlinear Growth, Saturation, and Gravitational Radiation,” *Phys. Rev. Lett.* **121**, 131104 (2018), [arXiv:1807.00043 \[gr-qc\]](#).
- [57] Valeri P. Frolov, Pavel Krtouš, David Kubizňák, and Jorge E. Santos, “Massive Vector Fields in Rotating Black-Hole Spacetimes: Separability and Quasinormal Modes,” *Phys. Rev. Lett.* **120**, 231103 (2018), [arXiv:1804.00030 \[hep-th\]](#).
- [58] Sam R. Dolan, “Instability of the Proca field on Kerr spacetime,” *Phys. Rev. D* **98**, 104006 (2018), [arXiv:1806.01604 \[gr-qc\]](#).
- [59] Richard Brito, Sara Grillo, and Paolo Pani, “Black Hole Superradiant Instability from Ultralight Spin-2 Fields,” *Phys. Rev. Lett.* **124**, 211101 (2020), [arXiv:2002.04055 \[gr-qc\]](#).
- [60] Hooman Davoudiasl, Peter B. Denton, and Julia Gehrlein, “Supermassive Black Holes, Ultralight Dark Matter, and Gravitational Waves from a First Order Phase Transition,” *Phys. Rev. Lett.* **128**, 081101 (2022), [arXiv:2109.01678 \[astro-ph.CO\]](#).
- [61] Adrian Ka-Wai Chung, Joseph Gais, Mark Ho-Yeuk Cheung, and Tjonnie G. F. Li, “Searching for ultralight bosons with supermassive black hole ringdown,” *Phys. Rev. D* **104**, 084028 (2021), [arXiv:2107.05492 \[gr-qc\]](#).
- [62] Yu-Mei Wu, Zu-Cheng Chen, Qing-Guo Huang, Xingjiang Zhu, N. D. Ramesh Bhat, Yi Feng, George Hobbs, Richard N. Manchester, Christopher J. Russell, and R. M. Shannon (PPTA), “Constraining ultralight vector dark matter with the Parkes Pulsar Timing Array second data release,” *Phys. Rev. D* **106**, L081101 (2022), [arXiv:2210.03880 \[astro-ph.CO\]](#).
- [63] Chen Yuan, Yang Jiang, and Qing-Guo Huang, “Constraints on an ultralight scalar boson from Advanced LIGO and Advanced Virgo’s first three observing runs using the stochastic gravitational-wave background,” *Phys. Rev. D* **106**, 023020 (2022), [arXiv:2204.03482 \[astro-ph.CO\]](#).
- [64] Asimina Arvanitaki, Masha Baryakhtar, and Xinlu Huang, “Discovering the QCD Axion with Black Holes and Gravitational Waves,” *Phys. Rev. D* **91**, 084011 (2015), [arXiv:1411.2263 \[hep-ph\]](#).
- [65] Richard Brito, Shrobona Ghosh, Enrico Barausse, Emanuele Berti, Vitor Cardoso, Irina Dvorkin, Antoine Klein, and Paolo Pani, “Stochastic and resolvable gravitational waves from ultralight bosons,” *Phys. Rev. Lett.* **119**, 131101 (2017), [arXiv:1706.05097 \[gr-qc\]](#).
- [66] Richard Brito, Shrobona Ghosh, Enrico Barausse, Emanuele Berti, Vitor Cardoso, Irina Dvorkin, Antoine Klein, and Paolo Pani, “Gravitational wave searches for ultralight bosons with LIGO and LISA,” *Phys. Rev. D* **96**, 064050 (2017), [arXiv:1706.06311 \[gr-qc\]](#).
- [67] Sylvia J. Zhu, Masha Baryakhtar, Maria Alessandra Papa, Daichi Tsuna, Norita Kawanaka, and Heinz-Bernd Eggenstein, “Characterizing the continuous gravitational-wave signal from boson clouds around Galactic isolated black holes,” *Phys. Rev. D* **102**, 063020 (2020), [arXiv:2003.03359 \[gr-qc\]](#).
- [68] Hideo Kodama and Hirotaka Yoshino, “Axiverse and Black Hole,” *Int. J. Mod. Phys. Conf. Ser.* **7**, 84–115 (2012), [arXiv:1108.1365 \[hep-th\]](#).

- [69] Richard Brito, Vitor Cardoso, and Paolo Pani, “Black holes as particle detectors: evolution of superradiant instabilities,” *Class. Quant. Grav.* **32**, 134001 (2015), [arXiv:1411.0686 \[gr-qc\]](#).
- [70] Leo Tsukada, Thomas Callister, Andrew Matas, and Patrick Meyers, “First search for a stochastic gravitational-wave background from ultralight bosons,” *Phys. Rev. D* **99**, 103015 (2019), [arXiv:1812.09622 \[astro-ph.HE\]](#).
- [71] Shoushan Bao, Qixuan Xu, and Hong Zhang, “Improved analytic solution of black hole superradiance,” *Phys. Rev. D* **106**, 064016 (2022), [arXiv:2201.10941 \[gr-qc\]](#).
- [72] Shou-Shan Bao, Qi-Xuan Xu, and Hong Zhang, “Next-to-leading-order solution to Kerr-Newman black hole superradiance,” *Phys. Rev. D* **107**, 064037 (2023), [arXiv:2301.05317 \[gr-qc\]](#).
- [73] Yin-Da Guo, Nayun Jia, Shou-Shan Bao, Hong Zhang, and Xin Zhang, “Evolution and detection of vector superradiant instabilities,” *Phys. Rev. D* **110**, 083029 (2024), [arXiv:2407.00767 \[gr-qc\]](#).
- [74] Giuseppe Ficarra, Paolo Pani, and Helvi Witek, “Impact of multiple modes on the black-hole superradiant instability,” *Phys. Rev. D* **99**, 104019 (2019), [arXiv:1812.02758 \[gr-qc\]](#).
- [75] Yin-da Guo, Shou-shan Bao, and Hong Zhang, “Subdominant modes of the scalar superradiant instability and gravitational wave beats,” *Phys. Rev. D* **107**, 075009 (2023), [arXiv:2212.07186 \[gr-qc\]](#).
- [76] Joseph Polchinski, “The Black Hole Information Problem,” in *Theoretical Advanced Study Institute in Elementary Particles* (2017) pp. 353–397, [arXiv:1609.04036 \[hep-th\]](#).
- [77] M. Yu. Kuchiev, “Reflection, radiation and interference for black holes,” *Phys. Rev. D* **69**, 124031 (2004), [arXiv:gr-qc/0310051](#).
- [78] M. Yu. Kuchiev, “Reflection from black holes,” (2003), [arXiv:gr-qc/0310008](#).
- [79] M. Yu. Kuchiev, “Reflection from black holes and space-time topology,” *EPL* **65**, 445–451 (2004), [arXiv:gr-qc/0310134](#).
- [80] M. Yu. Kuchiev and V. V. Flambaum, “Scattering of scalar particles by a black hole,” *Phys. Rev. D* **70**, 044022 (2004), [arXiv:gr-qc/0312065](#).
- [81] M. Yu. Kuchiev and V. V. Flambaum, “Reflection on event horizon and escape of particles from confinement inside black holes,” (2004), [arXiv:gr-qc/0407077](#).
- [82] V. V. Flambaum, “Tunneling into black hole, escape from black hole, reflection from horizon and pair creation,” (2004), [arXiv:gr-qc/0408013](#).
- [83] M. Yu. Kuchiev and V. V. Flambaum, “Causality condition and reflection on event horizon,” (2005), [arXiv:gr-qc/0502117](#).
- [84] Kostas Skenderis and Marika Taylor, “The fuzzball proposal for black holes,” *Phys. Rept.* **467**, 117–171 (2008), [arXiv:0804.0552 \[hep-th\]](#).
- [85] Hal M. Haggard and Carlo Rovelli, “Quantum-gravity effects outside the horizon spark black to white hole tunneling,” *Phys. Rev. D* **92**, 104020 (2015), [arXiv:1407.0989 \[gr-qc\]](#).

- [86] Eugenio Bianchi, Marios Christodoulou, Fabio D’Ambrosio, Hal M. Haggard, and Carlo Rovelli, “White Holes as Remnants: A Surprising Scenario for the End of a Black Hole,” *Class. Quant. Grav.* **35**, 225003 (2018), [arXiv:1802.04264 \[gr-qc\]](#).
- [87] Vitor Cardoso, Edgardo Franzin, and Paolo Pani, “Is the gravitational-wave ringdown a probe of the event horizon?” *Phys. Rev. Lett.* **116**, 171101 (2016), [Erratum: *Phys.Rev.Lett.* 117, 089902 (2016)], [arXiv:1602.07309 \[gr-qc\]](#).
- [88] Vitor Cardoso, Valentino F. Foit, and Matthew Kleban, “Gravitational wave echoes from black hole area quantization,” *JCAP* **08**, 006 (2019), [arXiv:1902.10164 \[hep-th\]](#).
- [89] Zachary Mark, Aaron Zimmerman, Song Ming Du, and Yanbei Chen, “A recipe for echoes from exotic compact objects,” *Phys. Rev. D* **96**, 084002 (2017), [arXiv:1706.06155 \[gr-qc\]](#).
- [90] Richard H. Price and Gaurav Khanna, “Gravitational wave sources: reflections and echoes,” *Class. Quant. Grav.* **34**, 225005 (2017), [arXiv:1702.04833 \[gr-qc\]](#).
- [91] Yun Fang, Rong-Zhen Guo, and Qing-Guo Huang, “Tests for the existence of horizon through gravitational waves from a small binary in the vicinity of a massive object,” *Phys. Lett. B* **822**, 136654 (2021), [arXiv:2108.04511 \[astro-ph.CO\]](#).
- [92] Shaunik Biswas, Mostafizur Rahman, and Sumanta Chakraborty, “Echoes from braneworld wormholes,” *Phys. Rev. D* **106**, 124003 (2022), [arXiv:2205.14743 \[gr-qc\]](#).
- [93] Pablo Bueno, Pablo A. Cano, Frederik Goelen, Thomas Hertog, and Bert Vercknocke, “Echoes of Kerr-like wormholes,” *Phys. Rev. D* **97**, 024040 (2018), [arXiv:1711.00391 \[gr-qc\]](#).
- [94] Taishi Ikeda, Massimo Bianchi, Dario Consoli, Alfredo Grillo, Josè Francisco Morales, Paolo Pani, and Guilherme Raposo, “Black-hole microstate spectroscopy: Ringdown, quasinormal modes, and echoes,” *Phys. Rev. D* **104**, 066021 (2021), [arXiv:2103.10960 \[gr-qc\]](#).
- [95] Jahed Abedi, Hannah Dykaar, and Niayesh Afshordi, “Echoes from the Abyss: Tentative evidence for Planck-scale structure at black hole horizons,” *Phys. Rev. D* **96**, 082004 (2017), [arXiv:1612.00266 \[gr-qc\]](#).
- [96] Rong-Zhen Guo, Chen Yuan, and Qing-Guo Huang, “Near-horizon microstructure and superradiant instabilities of black holes,” *Phys. Rev. D* **105**, 064029 (2022), [arXiv:2109.03376 \[gr-qc\]](#).
- [97] Rong-Zhen Guo, Chen Yuan, and Qing-Guo Huang, “On the interaction between ultralight bosons and quantum-corrected black holes,” *JCAP* **04**, 069 (2023), [arXiv:2301.06840 \[gr-qc\]](#).
- [98] Lihang Zhou, Richard Brito, Zhan-Feng Mai, and Lijing Shao, “Superradiant instabilities of massive bosons around exotic compact objects,” (2023), [arXiv:2308.03091 \[gr-qc\]](#).
- [99] Zhong-Hao Luo and Yun-Long Zhang, “Superradiant instability of area quantized Kerr black hole with discrete reflectivity,” (2024), [arXiv:2404.10742 \[gr-qc\]](#).
- [100] K. S. Thorne, “Multipole Expansions of Gravitational Radiation,” *Rev. Mod. Phys.* **52**, 299–339 (1980).
- [101] Oleg Lunin, “Maxwell’s equations in the Myers-Perry geometry,” *JHEP* **12**, 138 (2017), [arXiv:1708.06766 \[hep-th\]](#).

- [102] Pavel Krtouš, Valeri P. Frolov, and David Kubizňák, “Separation of Maxwell equations in Kerr–NUT–(A)dS spacetimes,” *Nucl. Phys. B* **934**, 7–38 (2018), [arXiv:1803.02485 \[hep-th\]](#).
- [103] Valeri P. Frolov, Pavel Krtous, and David Kubiznak, “Black holes, hidden symmetries, and complete integrability,” *Living Rev. Rel.* **20**, 6 (2017), [arXiv:1705.05482 \[gr-qc\]](#).
- [104] Emanuele Berti, Vitor Cardoso, and Andrei O. Starinets, “Quasinormal modes of black holes and black branes,” *Class. Quant. Grav.* **26**, 163001 (2009), [arXiv:0905.2975 \[gr-qc\]](#).
- [105] James M. Bardeen, William H. Press, and Saul A Teukolsky, “Rotating black holes: Locally nonrotating frames, energy extraction, and scalar synchrotron radiation,” *Astrophys. J.* **178**, 347 (1972).
- [106] J. D. Bekenstein, “Extraction of energy and charge from a black hole,” *Phys. Rev. D* **7**, 949–953 (1973).
- [107] Nils Siemonsen and William E. East, “Gravitational wave signatures of ultralight vector bosons from black hole superradiance,” *Phys. Rev. D* **101**, 024019 (2020), [arXiv:1910.09476 \[gr-qc\]](#).